UNDERSTANDING MOLECULAR INTERACTION BETWEEN SULFADOXINE AND HUMAN SERUM ALBUMIN THROUGH SPECTROSCOPIC AND MOLECULAR DOCKING METHODS

JASLENE ANNE A/P FRANCIS

FACULTY OF SCIENCE
UNIVERSITI MALAYA
KUALA LUMPUR

2021

UNDERSTANDING MOLECULAR INTERACTION BETWEEN SULFADOXINE AND HUMAN SERUM ALBUMIN THROUGH SPECTROSCOPIC AND MOLECULAR DOCKING METHODS

JASLENE ANNE A/P FRANCIS

DISSERTATION SUBMITTED IN FULFILMENT OF THE REQUIREMENTS FOR THE DEGREE OF MASTER OF SCIENCE

INSTITUTE OF BIOLOGICAL SCIENCES
FACULTY OF SCIENCE
UNIVERSITI MALAYA
KUALA LUMPUR

2021

UNIVERSITI MALAYA

ORIGINAL LITERARY WORK DECLARATION

Name of Candidate: **JASLENE ANNE A/P FRANCIS**
Matric No: **SMA180052**
Name of Degree: **MASTER OF SCIENCE**

Title of Dissertation ("this Work"):
UNDERSTANDING MOLECULAR INTERACTION BETWEEN SULFADOXINE AND HUMAN SERUM ALBUMIN THROUGH SPECTROSCOPIC AND MOLECULAR DOCKING METHODS

Field of Study: **BIOCHEMISTRY**

I do solemnly and sincerely declare that:

(1) I am the sole author/writer of this Work;
(2) This Work is original;
(3) Any use of any work in which copyright exists was done by way of fair dealing and for permitted purposes and any excerpt or extract from, or reference to or reproduction of any copyright work has been disclosed expressly and sufficiently and the title of the Work and its authorship have been acknowledged in this Work;
(4) I do not have any actual knowledge nor do I ought reasonably to know that the making of this work constitutes an infringement of any copyright work;
(5) I hereby assign all and every rights in the copyright to this Work to the University of Malaya ("UM"), who henceforth shall be owner of the copyright in this Work and that any reproduction or use in any form or by any means whatsoever is prohibited without the written consent of UM having been first had and obtained;
(6) I am fully aware that if in the course of making this Work I have infringed any copyright whether intentionally or otherwise, I may be subject to legal action or any other action as may be determined by UM.

Candidate's Signature Date: 20 / 01 / 2021

Subscribed and solemnly declared before,

Witness's Signature Date: 20 / 01 / 2021
Name:
Designation:

Witness's Signature Date: 20 / 01 / 2021
Name:
Designation:

UNDERSTANDING MOLECULAR INTERACTION BETWEEN SULFADOXINE AND HUMAN SERUM ALBUMIN THROUGH SPECTROSCOPIC AND MOLECULAR DOCKING METHODS

ABSTRACT

The main aim of this study was to characterize the molecular interaction between sulfadoxine (SDN) and the major transport protein in the blood plasma, human serum albumin (HSA) using fluorescence, absorption, circular dichroism and voltammetric techniques along with computational methods. SDN-induced changes in the fluorescence intensity of HSA hinted the complex formation between SDN and HSA. Both values of the bimolecular quenching rate constant and UV-Vis absorption spectral results characterized the quenching of HSA fluorescence as static quenching. Analysis of the quenching results showed a moderate binding affinity (K_a = 3.39×10^4 M^{-1} at 300 K) between SDN and HSA. Thermodynamic data (ΔS = + 104.42 J mol^{-1} K^{-1}, ΔH = + 5.25 kJ mol^{-1}) suggested participation of hydrophobic interactions as the main binding force in the complex formation. Secondary and tertiary structural changes along with microenvironmental perturbation around protein fluorophores were also noticed upon SDN binding. The voltammetric spectral analysis further supported the complex formation between HSA and SDN. Competitive ligand displacement results, as well as computational analysis, revealed binding of SDN to Sudlow's Site I, located in subdomain IIA of HSA.

Keywords: Sulfadoxine (SDN), human serum albumin (HSA), ligand-protein interaction, molecular docking, cyclic voltammetry.

MEMAHAMI INTERAKSI MOLEKULAR ANTARA SULFADOXINE DAN SERUM ALBUMIN MANUSIA MELALUI KAEDAH SPEKTROSKOPIK DAN DOK MOLEKUL

ABSTRAK

Tujuan utama kajian ini adalah untuk mencirikan interaksi molekul antara sulfadoxine (SDN) dan protein pengangkutan utama dalam plasma darah, serum albumin manusia (HSA) menggunakan pendarfluor, penyerapan, dikroism bulat dan teknik voltammetrik bersama dengan kaedah dok molekul. Perubahan yang disebabkan oleh SDN pada isyarat pendarfluor HSA mengisyaratkan pembentukan kompleks antara SDN dan HSA. Kedua-dua nilai kadar pendinginan bimolekular tetap dan keputusan spektrum penyerapan UV-Vis mencirikan pendinginan pendarfluor HSA sebagai pelindapkejutan statik. Analisis keputusan pelindapkejutan menunjukkan pertalian ikatan sederhana ($3.39 \times 10^4\ M^{-1}$ pada 300 K) antara SDN dan HSA. Data termodinamik (ΔS = + 104.42 J mol^{-1} K^{-1}, ΔH = + 5.25 kJ mol^{-1}) mencadangkan penyertaan interaksi hidrofobik sebagai daya pengikat utama dalam pembentukan kompleks. Perubahan struktur sekunder dan tersier bersama dengan gangguan lingkungan mikro di sekitar fluorofor protein juga diperhatikan pada pengikatan SDN. Analisis spektrum voltammetrik menyokong lagi pembentukan kompleks antara HSA dan SDN. Hasil pemindahan ligan yang kompetitif serta analisis dok molekul menunjukkan pengikatan SDN ke tapak I Sudlow, yang terletak di subdomain IIA HSA.

Kata kunci: Sulfadoxine (SDN), serum albumin manusia (HSA), interaksi protein-ligan, dok molekul, voltammetri siklik.

ACKNOWLEDGEMENTS

First, I would like to extend my deepest gratitude to my supervisors, Professor Saad Tayyab and Associate Professor Dr. Saharuddin Mohamad for their guidance and encouragement throughout the entire project. My special gratitude to Professor Saad Tayyab for his patience and support from the beginning of the project to the dissertation writing until the completion of this project. He was the only reason I managed to finish my project in the scheduled period.

I would also like to thank Associate Professor Dr. Zazali Alias, Coordinator of the Biochemistry Programme, Associate Professor Dr. Saharuddin Mohamad, Head, Institute of Biological Sciences and Professor Dr. Ismail Yusoff, Dean, Faculty of Science, University of Malaya for providing necessary facilities required for my research.

My special thanks to the University of Malaya for providing me the financial support in the form of Research Assistantship under Faculty Research Grant (GPF011B-2018), sanctioned to Professor Saad Tayyab.

I also take this opportunity to thank my colleagues, Amira Adlin Roslan, Salanee Kandandapani and Kabiru Abu Bakar Musa for their continuous support throughout the times we spent working together in the laboratory.

Last but not least, I am extremely thankful to my mother, Madam Agnes Arulapoo, sister, Diana Anne Francis and my entire maternal family for being there from the beginning and helping in all ways possible until to where I am now.

Jaslene Anne Francis

September, 2020.

TABLE OF CONTENTS

LIST OF FIGURES

LIST OF TABLES

LIST OF SYMBOLS AND ABBREVIATIONS

Å	:	Angstrom
℃	:	Degree Celsius
λ_{em}	:	Emission wavelength
λ_{ex}	:	Excitation wavelength
ΔH	:	Enthalpy change
ΔS	:	Entropy change
ΔG	:	Free energy change
>	:	Greater than
%	:	Percentage
Ala	:	Alanine
Arg	:	Arginine
CD	:	Circular dichroism
cm	:	Centimeter
3-D	:	Three-dimensional
Da	:	Dalton
DZM	:	Diazepam
Eq.	:	Equation
g/l	:	Gram per liter
Glu	:	Glutamic acid
His	:	Histidine
HMN	:	Hemin
HSA	:	Human serum albumin
i.e.	:	Latin abbreviations (in other words)
IgG	:	Immunoglobulin G
J	:	Joules

K	:	Kelvin
K_a	:	Binding constant
kJ	:	Kilojoules
K_{SV}	:	Stern-Volmer constant
k_q	:	Bimolecular quenching rate constant
Lys	:	Lysine
M	:	Molar
mg	:	Milligram
min	:	Minute
ml	:	Milliliter
mM	:	Millimolar
mm	:	Millimeter
nm	:	Nanometer
r	:	Correlation coefficient
sec	:	Second
Ser	:	Serine
SDN	:	Sulfadoxine
T	:	Temperature
Trp	:	Tryptophan
Tyr	:	Tyrosine
µA	:	Microampere
µM	:	Micromolar
UV	:	Ultraviolet
V	:	Voltage
viz.	:	Latin phrase *videlicet* (that is to say)
WFN	:	Warfarin

CHAPTER 1: INTRODUCTION

Malaria is one of the well-known parasitic diseases that affect millions of people in Africa, Asia and America (Central and South) with reports of ~ 212 million clinical cases in addition to 429 000 deaths annually (Choemang & Na-Bangchang, 2019). Among the annual death rates, children aged below 5 years form the most vulnerable group, susceptible to infection, as they account for ~ 67 % of the total death rate (WHO, 2020). This mosquito-borne disease is caused by *Plasmodium* species, in which the parasites multiply inside the human body when entered through the bites of infected female *Anopheles* mosquitoes (Tangpukdee et al., 2009). The human malaria is caused by five parasite species, namely, *Plasmodium falciparum*, *P. vivax, P. ovale, P. malariae* and *P. knowlesi*. Out of these five species, *P. falciparum* is known to cause immense threats (Tangpukdee et al., 2009). The multiplication of *Plasmodium* species is highly dependent on the availability of folate derivatives for nucleotide biosynthesis (Hyde, 2005; Nzila et al., 2005). The first antimalarial drug, chloroquine was found successful in inhibiting the survival of the malarial parasites due to interference with the folate metabolism (Gregson & Plowe, 2005). However, the inhibitory action of this drug was hampered due to mutations in the parasite (Le Bras & Durand, 2003). Due to the drug resistance developed by the malarial parasites against chloroquine, the emergence of several anti-malarial drugs in combination has been proved rewarding in treating malaria (Choemang & Na-Bangchang, 2019; Nzila et al., 2005).

Sulfadoxine (SDN) is a Food and Drug Administration (FDA)-approved drug, which is currently being used in combination with pyrimethamine in treating chloroquine-resistant malaria (Farrar et al., 2013). SDN inhibits the enzyme, dihydropteroate synthetase that is crucial to the parasitic folate biosynthetic pathway (Gatton et al., 2004). This helps in lowering the folic acid production, which is vital in the nucleic acid biosynthesis of the malarial parasite, hence inhibiting the parasite's mitotic division

(Saikia et al., 2017). Besides, SDN also participates in antibacterial action against infections of the respiratory organs, urinary and gastric tracts as well as osteomyelitis, sinusitis and other purulent infections (Vardanyan & Hruby, 2006).

The interaction study between a drug and plasma proteins is vital to understand a drug's distribution, metabolism, efficacy, half-life, stability and level of toxicity (Chi et al., 2010; Kragh-Hansen et al., 2002; Olson & Christ, 1996). The concentration of the free drug may change upon binding of several other compounds either to the same binding site on the transport protein or through allosteric effects, which can alter the drug toxicity level in the circulation (Bertucci & Domenici, 2002). Hence, the study on the interaction of a drug with the transport protein would be useful in understanding the drug's pharmacological properties and toxicity level in human circulation.

Human serum albumin (HSA) is the major transport protein for both endogenous and exogenous compounds, present in the human circulation. It is a single polypeptide chain, made up of 585 amino acid residues, which include a sole tryptophan residue (Trp-214). It is comprised of three structural domains (I, II and III), which are further divided into subdomains A and B (Carter et al., 1989; Peters, 1996; Sudlow et al., 1975). Besides, the protein has three high-affinity ligand binding sites, namely, Site I, Site II and Site III, which are located in the hydrophobic cavities of subdomains IIA, IIIA and IB, respectively (Sudlow et al., 1975).

Many techniques, *i.e.,* equilibrium dialysis (Nevídalová et al., 2018), UV-Vis absorption spectroscopy (Wani et al., 2018), spectrofluorimetry (Elgawish et al., 2019), circular dichroism (CD) spectroscopy (Baig et al., 2019), Fourier-transform infrared (FTIR) spectroscopy (Della et al., 2016), isothermal titration calorimetry (Feroz et al., 2016), potentiometry (Hosseinzadeh & Khorsandi, 2016) and dynamic light scattering (Yuan et al., 2017) are commonly used in studying the ligand-protein interaction. However, some of these methods have limitations such as long periods in

equilibrium dialysis and the nonselective nature of electrodes in the case of many ligands, such as drug molecules in the potentiometric method (Ayranci & Duman, 2004). On the other hand, fluorescence spectroscopy offers advantages of reproducibility, high sensitivity, cost-effectiveness and rapidity (Seedher & Bhatia, 2005; Yang et al., 2009).

Although the effects of SDN on treating human malaria have been widely studied (Kayentao et al., 2013; Mikomangwa et al., 2020; Terkuile et al., 2007), transportation of SDN in the human circulation through HSA binding has not been reported so far. Therefore, the problem statement and objectives of the present study were set in the following way.

Problem statement: Does SDN bind to the major carrier protein in human circulation, *i.e.,* human serum albumin (HSA)? If yes, what are the binding characteristics of SDN-HSA interaction?

To answer the above question, following objectives were laid down:

- To study the interaction of SDN with HSA in terms of binding affinity and binding forces.
- To monitor the electrochemical changes of HSA upon SDN binding.
- To evaluate protein's secondary and tertiary structures as well as microenvironmental perturbation around protein's fluorophores in the presence of SDN.
- To examine the thermal stability of HSA upon SDN binding, and
- To identify the SDN binding site on HSA.

To achieve the above objectives, binding studies of SDN with HSA were made using several spectroscopic, voltametric and computational approaches.

CHAPTER 2: LITERATURE REVIEW

2.1 Malaria

Over the years, malaria has been the most life-threatening disease, claiming around 150–300 million lives annually, as observed during the period 2013–2018, especially in locations such as sub-Saharan Africa, Asia, the Amazon basin and other tropical regions (WHO, 2018). Figure 2.1 displays the malaria transmission around the world during 2017–2020 in which Malaysia has been marked as the region where malaria transmission occurs in some places. Although the distribution of the disease covers vast areas, the burden has been detected heaviest in the African Region, where an estimated 93% of all malaria deaths occur annually (WHO, 2018).

Malaria is caused by malarial parasite, a single-celled protozoan, which infects female *Anopheles* mosquitoes and is then transmitted into the human body through the bites of infected mosquitoes (Massele et al., 1993). The initial discovery of the parasite was linked with swamps responsible for the spread of Roman fever, which inspired the name mal'aria ("bad air"). Later, the finding of a clear, circular body containing malarial pigment in an *Anopheles* mosquito, resembling similar observation in infected humans confirms the transmission of the parasite between *Anopheles* mosquitoes and human (Jarcho, 1984). The rapid replication of the parasites in the human body produces initial symptoms like high fever, vomiting, headache and muscle pain and if left untreated, leads to fatality like severe anaemia, jaundice, kidney failure, etc. (Massele et al., 1993). On the other hand, the inoculation of malarial parasites among other female *Anopheles* mosquito occurs when they bite an infected human (Gelband et al., 2004).

The human malaria was caused by four *Plasmodium* species, namely, *P. vivax*, *P. falciparum*, *P. malariae* and *P. ovale* (Coombs et al., 2001; Gelband et al., 2004; Laveran et al., 1982). *Plasmodium vivax*, which is widespread in temperate as well as tropica

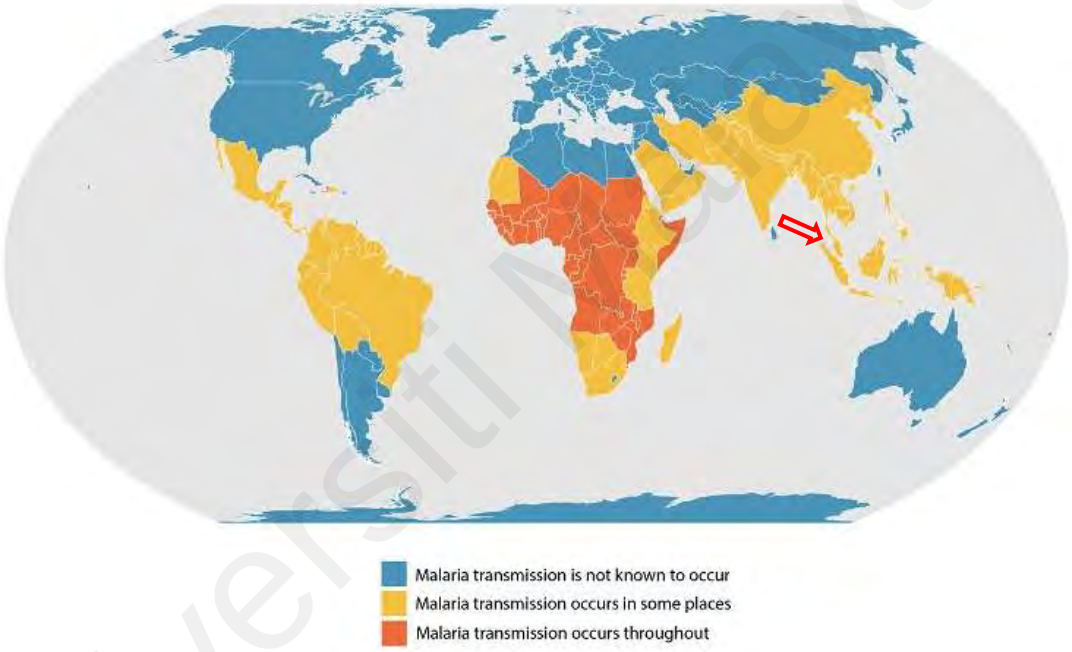

Figure 2.1: The mortality rate caused by malarial parasite around the world. Arrow is representing Malaysia which shows transmission of parasites at certain places. (Photo sourced from www.cdc.gov).

subtropical zones have the widest geographical range because it can survive at lower temperatures inside a mosquito than the other three parasites that infect humans. *Plasmodium falciparum*, the most lethal strain is the most prevalent species throughout the tropics and subtropics. *Plasmodium malariae* is patchily present over the same range as *P. falciparum*. *Plasmodium ovale* is found in tropical Africa, and occasionally in Asia, and the western Pacific (Gelband et al., 2004). Contrarily, the emergence of the fifth malarial parasite, *P. knowlesi* was discovered in East Malaysia in the year 2004 (Singh et al., 2004). This parasite has been reported to infect human through the forest macaques, found in the rural areas (Cox-Singh & Singh, 2008).

2.1.1 Malarial parasite life cycle

The life cycle of the malarial parasite involves two hosts: female *Anopheles* mosquito and human. Its life cycle is divided into three stages, as shown in Figure 2.2. These are the 'mosquito stage', 'human liver stage', and 'human blood stage' (Gelband et al., 2004). When a malaria-infected female *Anopheles* mosquito bites a human, the mosquito inoculates sporozoites into the human host, which then induces infection into the liver cells. The initial replication occurs in the liver where the sporozoites mature into schizonts, which are then released into the human blood as merozoites. Later, the parasites undergo asexual multiplication in the erythrocytes where, the merozoites grow inside the red blood cell, causing damage to them, and the cycle repeats as they invade other red blood cells (Gelband et al., 2004; Tuteja, 2007). At the same time, some of the parasites might differentiate into sexual gametocytes.

In the blood stage, parasites show symptoms of malaria. Both the male and the female gametocytes are ingested by an uninfected female *Anopheles* mosquito that bites the infected human. The parasites then, multiply itself in the mosquito host, called as

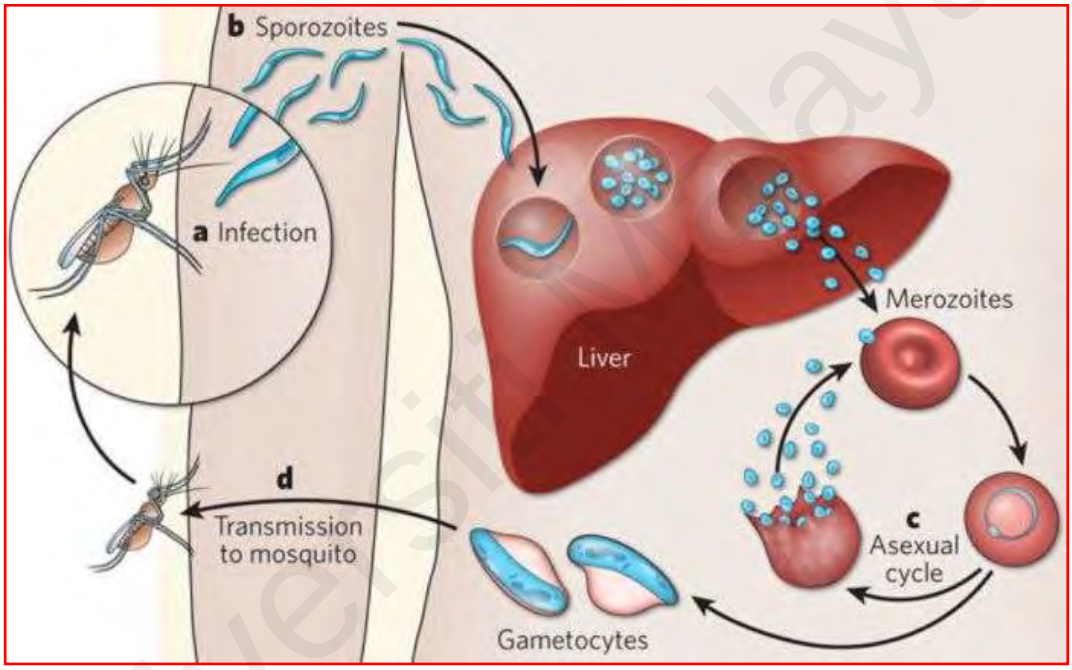

Figure 2.2: The lifecycle of a malarial parasite, representing three different stages; *i.e.*, mosquito, human liver and human blood. (Copyright permission from Springer Nature).

sporogonic cycle. Hence, the cycle repeats as the mosquito, carrying the parasite infects another human host (Tuteja, 2007).

However, the transmission of malaria can also be induced through the transfusion of malaria-tainted blood products or the contaminated red blood cells / tissues in the bone marrow or transplanted organs (Takem & D' Alessandro, 2013).

2.1.2 Early reactions towards *Plasmodium falciparum* in adults and children

Among the four malarial parasites that infect humans, *P. falciparum* is the most virulent and poses the greatest risk of complications and death (Greenwood & Mutabingwa, 2002; McGregor, 1974). *Plasmodium falciparum* gives rise to a broad spectrum of disease from asymptomatic infection to fatal syndromes such as cerebral malaria, severe anaemia, and multi-organ failure (WHO, 2000). In areas of high transmission of malaria caused by *P. falciparum* such as in Africa, functional immunity is acquired in two stages, *i.e.,* the initial phase of clinical immunity, followed by anti-parasite immunity. This helps in limiting the parasite numbers, replication, and burden within the human host (Schofield, 2002). In other words, functional immunity results in a progressive ability to contain malaria parasitaemia. On the other hand, human and parasite genetic variability, parasite-induced immunosuppression and other factors also contribute to the final degree of protection (Mohan & Stevenson, 1998).

There is a grace period when infants born to functionally immune mothers, transplacental antibody (maternal IgG) confers relative resistance to infection, and severe clinical episodes of malaria for the first six months of life (Edozien et al., 1962). High levels of fetal hemoglobin also offer partial protection (Pasvol et al., 1976). Over the next few years, children exhibit enhanced susceptibility to severe and fatal malaria caused by *P. falciparum* (Marsh, 1992). This early clinical immunity is sometimes referred to as 'clinical tolerance', signifying the ability to remain asymptomatic despite a relatively high

frequency of being bitten by the mosquitoes. However, the immunity drops in older-age individuals, leading to a rise in malaria cases caused by *P. falciparum* (Carter & Mendis, 2003). This has prompted the scientific community for the discovery of antimalarial drugs to assist in combating malarial infection (Bunnag et al., 1996).

2.1.3 The emergence of antimalarial drugs

With the simultaneous development of functional immunity, the discovery of the first antimalarial drug, chloroquine was found to be effective in fighting against *P. falciparum*. The drug functions by accumulating itself in the vacuole of *P. falciparum* and preventing haemoglobin degradation (Loeb et al., 1946). However, chloroquine resistance was noticed in the early 1960s at the Colombian-Venezuelan border (Moore & Lanier, 1961), and then towards sub-Saharan Africa in 1988 and South East Asia starting early 2000s (Ridley, 2002). Later, the discovery of several new antimalarial drugs such as mefloquine, halofantrine, sulfadoxine, pyrimethamine, etc. was also made to compensate chloroquine resistant malarial infection caused by *P.falciparum* (Cosgriff et al., 1982; Foley & Tilley, 1997; Kapoor, 1988). However, individual functions of these drugs were found to result in resistance after their usage for some time, which brought to the development of artemisinin to fight against the parasite (Eastman & Fidock, 2009). Artemisinin was found to be efficacious against all multi-drug resistant forms of *P. falciparum*. Besides, the use of artemisinins has become integral in the fight against malaria with artemisinin-based combination therapy (ACT), making up most modern-day treatments (Eastman & Fidock, 2009).

2.1.4 Classification of antimalarial drugs

The antimalarial drugs (Table 2.1) were classified into a single or combined therapy (Eyasu, 2015; Gelband et al., 2004).

Table 2.1: Classification of antimalarial drugs according to regimen. (Copyright permission from Toxicological International).

	Category	Examples
Single antimalarial drugs	Cinchona alkaloid	Quinine and Quinidine
	4-Aminoquinolines	Chloroquine, Amodiaqine, and Piperaquine
	8-Aminoquinolines	Primaquine and Bulaquine
	Diaminopyrimidines	Pyrimethamine
	Sulfonamide and Sulfone	**Sulfadoxine**, Sulfamethopyrazine, and Dapsone
	Sesquiterpine lactones	Artesunate, Artemeter, and Arteether
	Quinoline-methanol	Mefloquine
	Tetracyclines	Tetracycline and Doxycycline
	Amino alcohols	Halofantrine and Lumefantrine
	Mannich base	Pyronaridine
	Napthoquinone	Atorvaquone
	Biquanides	Proguanil and Chlorproguanil
Combination therapies	Non- artemisinin	(Sulfadoxine + Pyrimethamine), (Sulfadoxine + Pyrimethamine + Chloroquine), (Sulfadoxine + Pyrimethamine +Amodiaquine), (Sulfadoxine + Pyrimethamine + Mefloquine), (Quinine +Tetracycline), (Quinine + Doxycycline)
	Artemisinin	(Artesunate + Amodiaquine, Artesunate + Mefloquine, (Artemether + Lumefantrine), (Artesunate + Sulfadoxine/Pyrimethamine), (Dihydroartemisinin + Piperaquine), (Artesinin + Piperaguine + Primaquine) and (Pyronaridine + Artesunate)
Other combinations		(Chlorproguanil + Dapsone + Artesunate), (Arterolane maleate + Piperaquine phosphate)

A single antimalarial drug therapy involves the use of a single drug to control and eliminate malaria. This functions as monotherapy against uncomplicated malaria (Mendis et al., 2009). The single antimalaria agents can be divided based on their chemical structures and mode of action *i.e*., aryl aminoalcohol compounds and antifolate compounds (Gelband, 2004). The single therapy antimalarial drugs differ considerably in their pharmacokinetics in terms of their efficacy, dosage, and duration of treatment. Furthermore, the drug response was also found to vary among people. Some of these responses can be genetically determined, others by health status or by dietary factors (Gelband, 2004).

On the other hand, combination therapy involves the additive potential of two or more drugs, which have an independent mode of actions and different target sites to function in improving the therapeutic effect and development of the resistance towards malaria. The combination therapy of multiple antimalarial drugs is divided into artemisinin and non-artemisinin combination (Erhirhie, 2006).

Artemisia annua, or sweet wormwood plant is the source of artemisinin and its derivatives *i.e*., artesunate, artemether, artesinin, which are well known for their ability to swiftly reduce the number of *Plasmodium* parasites in the blood of patients (Klayman et al., 1984). The combination of artemisinin with the antimalarial drugs provides a quicker action against the proliferation of different stages of the parasites as well as *in vivo* activity (Terkuile et al., 1993; White 1997). The artemisinin-combination drugs play important roles in multi-drug resistance of *P. falciparum,* as they are not only active against the mature ring stage of *P. falciparum*, when the parasite is highly metabolically active, but also targets the young ring stages of the parasite. This offers a rapid reduction of the parasite biomass and may help in the reduction of the resistant alleles, which may reduce the gametocyte carriage (Okell et al., 2008).

Alternatively, non-artemisinin combination of antimalarial drugs involves the combination of the first line or the second line drugs used for the treatment against *P. falciparum*. These include drugs that have individual functions against the parasites but are almost similar in their pharmacokinetic properties to be used as the combination therapy (Whegang et al., 2010). This non artemisinin-based combination therapy is reserved as an interim option for countries, which are unable immediately to move to artemisinin combination of antimalarial drugs (Bloland, 2003; Whehang et al., 2010).

Among several non-artemisinin combination uses of antimalarial drugs, sulfadoxine seems to be the most prevalent due to its profound function in regions, where artemisinin combination therapy is not available. The inexpensive and wide availability of sulfadoxine promotes its usage to treat malaria in these regions (Bloland, 2003).

2.2 Sulfadoxine

Sulfadoxine (SDN), whose chemical structure is given in Figure 2.3, has been found as a better substitute for chloroquine in controlling malarial parasite. It is synthesized from methyl ester of methoxyacetic acid and has a solubility of 2.96×10^{-1} g/l (Aucamp et al., 2016). Sulfadoxine is characterized as an aminobenzenesulfonamide, which contains a benzenesulfonamide moiety with an amine group attached to it (Kapoor, 1988). It functions mainly to compete with para-aminobenzoic acid (pABA) in order to inhibit the bacterial enzyme, dihydropteroate synthase (DHPS) in the nucleic acid biosynthesis of malarial parasite (Figure 2.4). The inhibition of parasitic folic acid synthesis and de novo synthesis of purines and pyrimidines ultimately result in cell growth arrest and cell death (Sirichaiwat et al., 2004).

The use of SDN for the intermittent preventive treatment during pregnancy for mother's affected with malaria disease has been widely recognized (De Kock et al., 2017; Deloron et al., 2010; Newman et al., 2003). The impact of SDN has been found to reduce

A

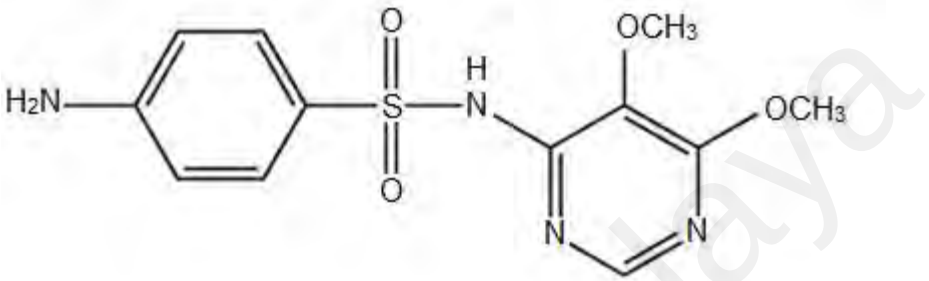

B

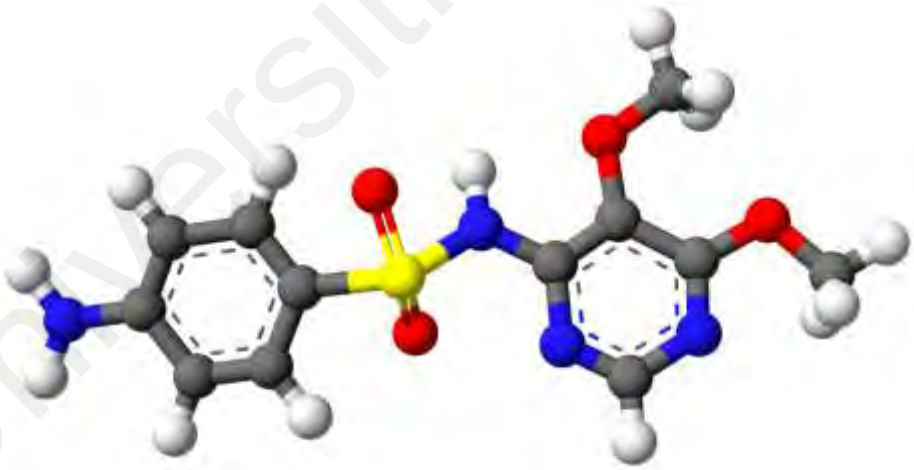

Figure 2.3: Chemical structure (A) and ball-and-stick model (B) of SDN.

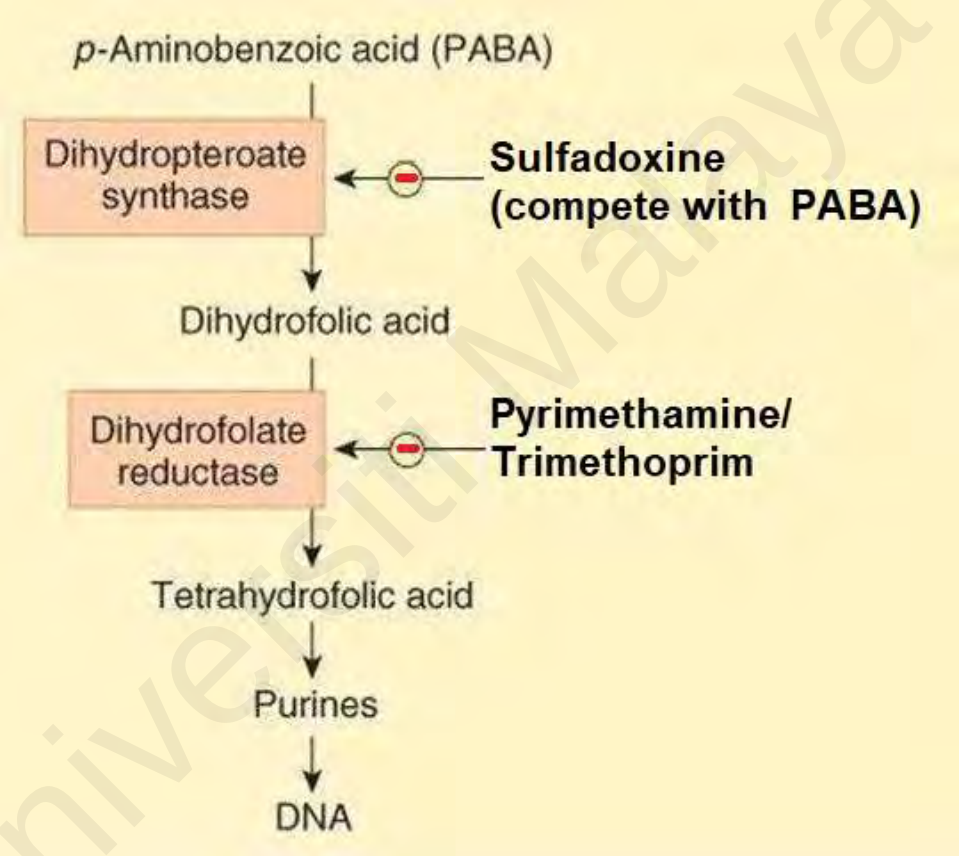

Figure 2.4: Schematic diagram showing inhibition of enzymes, of the parasite folate synthesis pathway by sulfadoxine, pyrimethamine and trimethoprim. (Copyright permission from McGraw-Hill Education).

the prevalence of histopathological placental malaria and improve the birth weight (Mlugu et al., 2020). The function of SDN has also been reported as an anti-infective agent against respiratory and urinary tract infections (Philips-Howard & Wood, 1996).

Sulfadoxine is being used in combination with several other drugs (Table 2.1) in combating malaria disease (Aronson, 2003; Chulay et al., 1984; Mutabingwa et al., 2005). Its application in the artemisinin-based combination therapy has been found effective than as a single drug, which leads to poorer adherence due to it's longer half-life of ~ 184 hours (Gatton et al., 2004). The combination therapy of SDN with other antimalarial drugs helps in reducing the parasite density in lesser time, which significantly lowers the parasite exposure to subtherapeutic blood levels (White, 1997). The frequent combination of SDN with pyrimethamine (Fansidar) has been proven as an effective replacement of chloroquine drug to fight against malaria, caused by *P. falciparum* (Terlouw et al., 2003). Its combination with amodiaquine and pyrimethamine has also been widely practiced as artemisinin-based combination therapy to reduce the risk of further resistance, developing towards uncomplicated malaria (Sinclair et al., 2009). Besides, SDN has also been recognized as an antibacterial agent in combination with trimethoprim with an advantage of its low-cost production (Maddison et al., 2008).

2.3 The importance of drug-protein interaction

When therapeutic drugs enter the human circulation, they will be carried by various transport proteins to their target sites. The interaction between the exogenous drugs and transport proteins might alter the drug's solubility, pharmacokinetics (absorption, metabolism, distribution and elimination), pharmacodynamics, therapeutic impact as well as toxicity level in the human circulation (Kragh-Hansen et al., 2002; Peters, 1996). Besides, the protein-bound drugs are protected against metabolism of the detoxification process, occurring in the body as well as reducing the concentration of their free form in

the circulation (Lindup & Orme, 1981). The drug-protein interaction study will help in choosing the optimal dosage prescription and further lead in understanding various responses of an individual in a drug therapy (Jamei et al., 2009). Therefore, in terms of the human health, the drug-albumin interaction study may provide useful information for a safer and an efficient therapy as well as in the diagnosis at the clinical level (Larsen et al., 2016; Yamasaki et al., 2013). Being the most abundant transport protein in the human circulation, the interaction mechanism of human serum albumin (HSA) with several antimalarial drugs has been previously documented (Ma et al., 2019; Musa et al., 2020; Yadav et al., 2020). The binding characteristics of these antimalarial drugs to HSA revealed significant differences. For instance, piperaquine showed a stronger binding affinity to HSA while lumefantrine and dispiro-tetraoxanes were bound to the protein through a moderate binding affinity. Furthermore, the interaction forces, involved in drug-HSA complex formation also showed variation. Besides, the binding sites of these drugs were found different in their preference as either Site I or Site II or both Site I and Site II of HSA (Ma et al., 2019; Musa et al., 2020; Yadav et al., 2020). These differences suggest that the binding characteristics of antimalarial drugs to HSA control their half-life, bioavailability and distribution upon binding to HSA. However, the data on SDN's transportation, pharmacokinetics, and bioavailability has not been discussed previously. This has made the interaction study between SDN and HSA crucial, as it can provide information to assist in understanding the pharmacology and toxicity of SDN.

2.4 Human serum albumin

Human serum albumin (HSA) is synthesized in liver from a single gene in the form of preproalbumin (Dugaiczyk et al., 1982). With the cleavage of the N-terminal peptide (pre-peptide) of the nascent chain, it is then released from the rough endoplasmic reticulum as proalbumin. The product is again cleaved at its N-terminal end (pro-peptide) in the Golgi apparatus to produce secreted albumin (Peters & Davidson, 1982). Serum albumin is a

member of a group of homologous proteins such as α-fetoprotein, afamin, and vitamin D binding protein (Fasano et al., 2007; Peters, 1996) which possess distinctive features to facilitate ligand binding. Human serum albumin is the predominant protein in the blood plasma and constitutes for more than 50 % of the total plasma protein content (Quinlan et al., 2005). The remaining albumin is distributed in the extracellular locations such as skin, muscle and other body fluids (cerebrospinal, pleural, peritoneal, pericardial, amniotic fluids, etc) as well as secretions including milk, sweat, tears and saliva (Quinlan et al., 2005).

2.4.1 Physicochemical properties of HSA

Table 2.2 shows some of the physicochemical properties of HSA. Human serum albumin has a molecular mass of ~ 66 kDa, as obtained from the amino acid composition (66 438 Da) as well as matrix-assisted laser desorption / ionization-time of flight (MALDI-TOF) mass spectrometry (66 479 Da) (Dockal et al., 1999; Peters, 1996). Based on the x-ray crystallographic results, the 3–D equilateral triangle shape of HSA was described with a side of 80 Å and a depth of 30 Å (He & Carter, 1992). Although HSA is known to possess a heart-shaped tertiary structure, but it is spheroid when placed in a solution (Quinlan et al., 2005). The protein was found to poses axial ratio of 3:1 of HSA, as predicted from the frequency dispersion of the dielectric constant (Scheider et al., 1976). A value of 26.7 Å was suggested for the radius of gyration (Carter & Ho, 1994). The globular conformation of HSA was prescribed based on its frictional ratio of 1.28:1 and its intrinsic viscosity of 0.040 dl g^{-1} (Jirgensons, 1955; Oncley et al., 1947). The protein isoelectric point was found to be 4.7 for fatted HSA while and 5.8 in the fatty acid free form (Peters, 1996). The protein possesses a net charge at pH 7.4 as –19, which supports its high solubility in aqueous environment. The isoionic point of HSA is 5.16 (Putnam, 1975) and it has an extinction coefficient of 5.3 at 280 nm (Wallevik, 1973). The conformation of HSA is mainly contributed by α-helical structure, accounting for

Table 2.2: Physicochemical properties of HSA.

Property	Value	Reference
Molecular mass		
- Amino acid composition	66 438 Da	Peters (1996)
- MALDI-TOF	66 479 Da	Dockal et al. (1999)
Diffusion coefficient, $D_{20,W}$	6.1×10^{-7} cm^2 s^{-1}	Oncley et al. (1947)
Sedimentation coefficient, $S_{20,W}$	4.2 S	Hunter & McDuffie (1959)
Frictional ratio, f/f_0	1.28:1	Oncley et al. (1947)
Axial ratio	3:1	Scheider et al. (1976)
Radius of gyration	26.7 Å	Carter & Ho (1994)
Overall dimension	80 × 80 × 30 Å	He & Carter (1992)
Intrinsic vicosity, $[\eta]$	0.0460 dl g^{-1}	Jirgensons (1955)
Partial specific volume, $\bar{v}_2$	0.733 cm^3 g^{-1}	Hunter (1966)
Isoelectric point		
- Native	4.7	Peters (1996)
- Defatted	5.8	Peters (1996)
Isoionic point	5.16	Putnam (1975)
Net charge (pH 7.4)	–19	Tanford (1950)
$\epsilon^{1\,\%}_{1\,cm}$ at 280 nm	5.3	Wallevik (1973)
Secondary structures		
- α-helix	67 %	Carter & Ho (1994)
- β-form	10 %	Carter & Ho (1994)

67 % secondary structure, while the rest of the residues are folded into β-pleated sheets (10 %) and flexible regions (23 %) between subdomains (Carter & Ho, 1994).

2.4.2 Structural characteristics of HSA

The amino acid composition of HSA is shown in Table 2.3. The protein is characterized by the presence of a single Trp residue, while large number of charged amino acid residues, *i.e.,* His (16), Arg (24), Asp (36), Glu (62) and Lys (59) contribute towards its aqueous solubility. Besides, hydrophobic amino acid residues are also broadly distributed, *i.e.,* Ala (62), Leu (61), Phe (31), Pro (24) and Val (41). The sulphur containing amino acids are distributed as 35 Cys and 6 Met residues. The amino acid sequence of HSA is shown in Figure 2.5, which is made up of a single polypeptide chain of 585 amino acid residues. These residues are grouped together under nine loops through seventeen disulphide bridges. These loops are further organized into three homologous domains, namely I, II and III, in which each domain is made up of two larger loops and one shorter loop. The domains I, II and III consist of amino acid residues from 1–195, 196–383, and 384–585, respectively (Peters, 1996). These domains are further divided into two subdomains 'A' and 'B'. The subdomains IA, IIA and IIIA are made up of the first two loops of each domains, 1–2, 4–5, and 7–8, respectively. On the other hand, subdomains IB, IIB and IIIB were characterized by the loops 3, 6 and 9, respectively (Peters, 1996). The subdomains 'A' and 'B' consist of six and four α-helices, respectively, which have similar patterns of helices h1–h4 in both the subdomains. However, two additional short helices (h5 and h6) are the part of subdomain A (Figure 2.6). Out of 35 cysteine residues, 34 are engaged in the formation of seventeen disulphide bridges while the lone Cys residue (Cys-34) is localised in subdomain IA. The arrangement of the six subdomains is shown in Figure 2.7.

Table 2.3: Amino acid composition of HSA. (Adapted from: Peters (1996)).

Amino acid	Number of residues
Alanine	62
Arginine	24
Asparagine	17
Aspartic acid	36
Cysteine	35
Glutamic acid	62
Glutamine	20
Glycine	12
Histidine	16
Isoleucine	8
Leucine	61
Lysine	59
Methionine	6
Phenylalanine	31
Proline	24
Serine	24
Threonine	28
Tryptophan	1
Tyrosine	18
Valine	41
Total	**585**

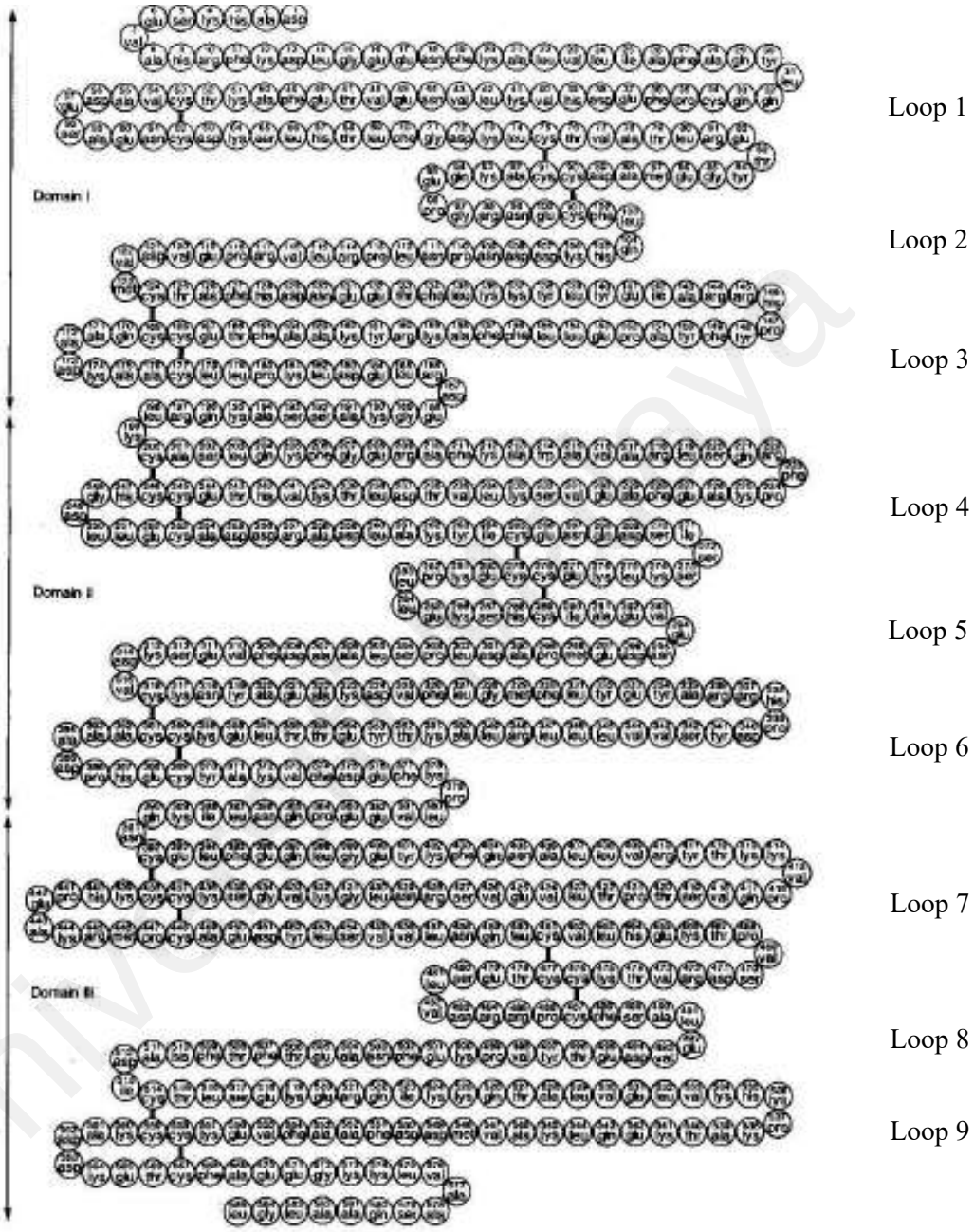

Figure 2.5: Amino acid sequence and disulphide bonding pattern of HSA. The serpentine layout of the polypeptide chain was according to Brown, 1976. (Copyright permission from Proceedings of the National Academy of Sciences of the United States of America).

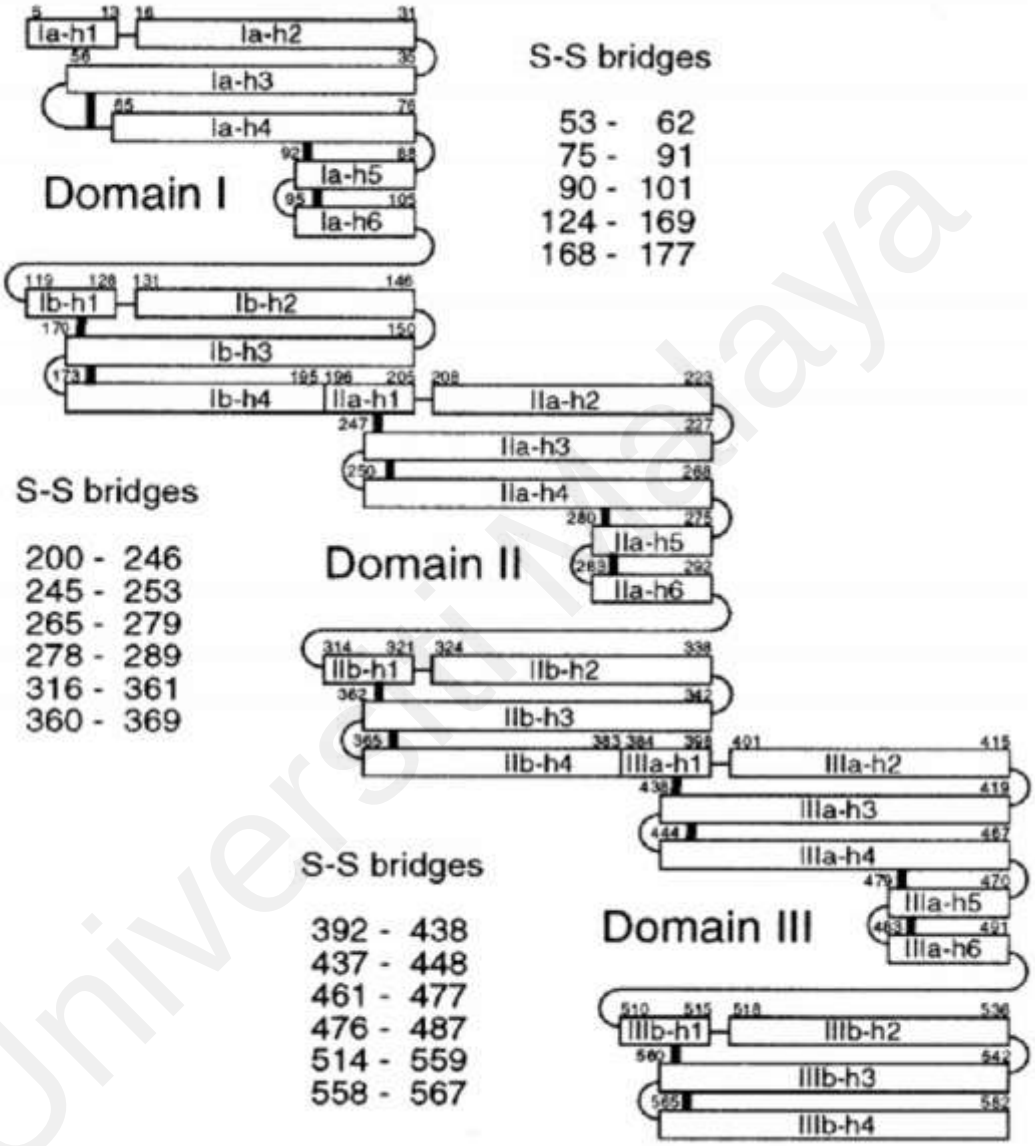

Figure 2.6: Diagram of helices and disulphide bridges of HSA. Helices are represented by rectangles, thin lines indicates the loops and turns, whereas, thick lines shows the disulphide bridges. The nomenclature was obtained from Minghetti et al. (1986). (Copyright permission from Oxford University Press).

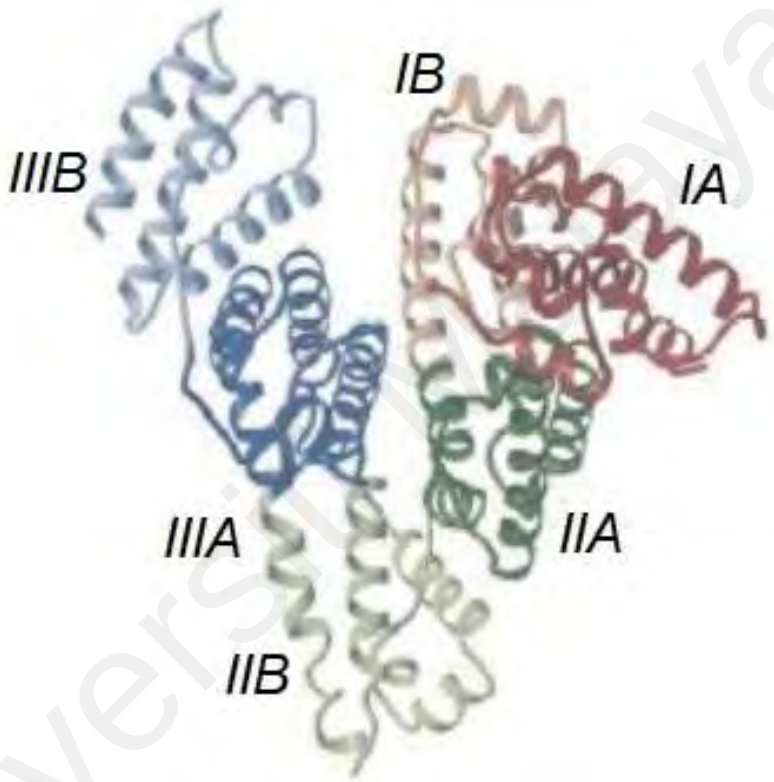

Figure 2.7: Three-dimensional structure of HSA showing six subdomains, coloured with six different colours. (Copyright permission from Elsevier).

2.4.3 Functions of HSA

Serum albumin is well known for its ligand binding properties, and its ability to transport large number of ligands, which include both exogenous and endogenous compounds, *i.e.,* bile salts, fatty acids, amino acids, etc. Besides, HSA carries metal ionsin the blood circulation such as zinc, iron, calcium, copper and chloride ions (Kragh-Hansen et al., 2002; Peters, 1996). It also transports therapeutic drugs and toxic compounds (Kragh-Hansen et al., 2002). Serum albumin has also been documented to function as antioxidant in protecting protein-bound compounds from oxidative damage (Roche et al., 2008) as well as possessing enzymatic (esterase) activity (Goncharov et al., 2017). Being the most abundant protein, HSA functions in the maintenance of blood pH and osmotic pressure regulation (Figge et al., 1991; Peters, 1996).

2.4.4 Binding sites of HSA

Binding of various ligands to different binding sites of HSA has been reported (Curry, 2009; Peters, 1996). According to Sudlow and his group (Sudlow et al., 1975), there are two well characterised ligand binding sites, known as Sudlow's Site I and Site II, respectively. Based on the enzymatic digestion results, their location has been identified to be in subdomain IIA and IIIA, respectively (Figure 2.8) (Bos et al., 1988; Sudlow et al., 1975). However, a third binding site in HSA, located in subdomain IB (Figure 2.8) has also been recognized (Carter et al., 2007). A further information about these binding sites is given below.

2.4.4.1 Site I

Site I of HSA is comprised of a pair of non-polar clusters which are joined together by two-centrally located clusters (at the entrance and at the bottom) of polar residues. At the entrance, the amino acid residues of Lys-195, Lys-199, Arg-218 and Arg-228 are accumulated, whereas Tyr-150, His-242 and Arg-257 gathers at the bottom of the pocket

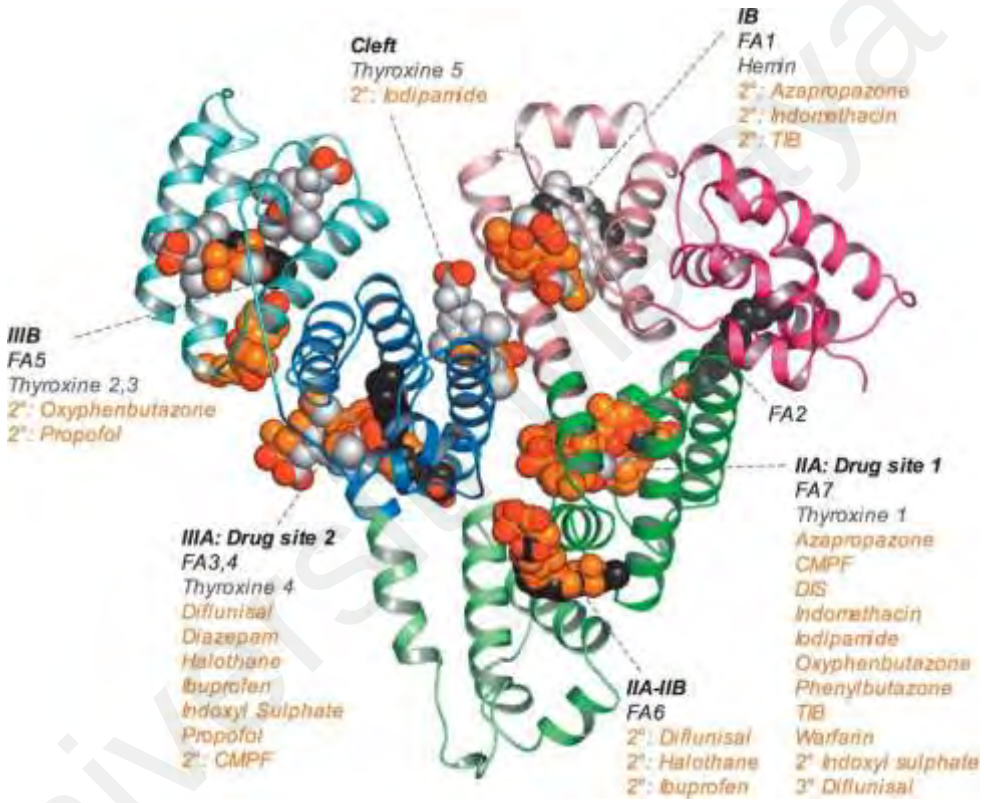

Figure 2.8: Structure of HSA showing location of different drug binding sites. The subdomains are coloured differently to distinguish the ligands which are filled as a space-filling models. (Copyright permission from Elsevier).

(Ghuman et al., 2005). Site I has been documented as a preferred binding site of bulky heterocyclic compunds, *viz.* warfarin, phenylbutazone and azapropazone (Ghuman et al., 2005; Kragh-Hansen et al., 2002; Sudlow et al., 1975). However, due to the mutual interaction between warfarin and azapropazone, their binding to Site I have been reported to be overlapping (Fehske et al., 1982). Therefore, presence of two-independent binding regions at Site I of HSA has been reported by Kragh-Hansen (1985; 1988).

2.4.4.2 Site II

Site II of HSA is characterized as nonpolar in nature due to the presence of hydrophobic side chains and double disulphide bridges of helix IIIa-h3 that lined up the pocket. Interior of the binding pocket is mostly hydrophobic with a single dominant polar patch, cantered around the hydroxyl group of Tyr-411, which faces toward the inside of the pocket and Arg- 410, which is located at the entrance of the pocket (Sugio et al., 1999). The size of Site II is smaller as compared to Site I, which prevents the involvement of overlapping binding sites as in Site I. This also induced a lesser flexibility in the binding of ligands, which indicates the binding of ligands to Site II is influenced by stereoselectivity (Kragh-Hansen et al., 2002). For instance, diazepam is known to bind to Site II of HSA but the binding of fluorinated diazepam was hampered (Chuang & Otagiri, 2001).

2.4.4.3 Site III

The third binding site of HSA, *i.e.,* Site III (non classical binding site) was discovered by Carter et. al. (2007; 2010) who claimed subdomain IB to be third-major drug binding site. The hydrophobic cavity of the Site III consist of three basic residues at its entrance and the binding pocket is partly blocked by Tyr-138 and Tyr-161 residues in the absence of ligand (Zunszain et al., 2003). The binding of ligand at the D-shaped cavity of Site III includes, hemin, digitoxin, and tamoxifen (Ojingwa et al., 1994; Zsila, 2013).

In reference to the pharmacological importance of SDN and HSA, SDN interaction with HSA is yet to be explained in terms of binding affinity, forces involved in the interaction, microenvironmental changes around protein fluorophores, electrochemical changes, and thermal stability of HSA and its binding site on HSA. These binding characteristics were studied using different spectroscopic and computational modelling methods which are explained in further sections.

CHAPTER 3: MATERIALS AND METHODS

3.1 Materials

3.1.1 Protein, drug and site markers

Essentially fatty acid-free human serum albumin (HSA) (purity>99%; Lot #068K7538V), sulfadoxine (SDN) (purity>95%; Lot #BCBS4285V), warfarin (WFN) (purity>98%; Lot #104K1261) and hemin (HMN) (purity>80%; Lot #015K0872) were procured from Sigma-Aldrich Co., St Louis, MO, USA. Diazepam (DZM) (purity>98%; Lot #1071B02) was purchased from Lipomed AG, Arlesheim, Switzerland.

3.1.2 Other chemicals/materials

Sodium dihydrogen phosphate and *di*-sodium hydrogen phosphate were purchased from SYSTERM®, Selangor, Malaysia. Dimethyl sulphoxide (DMSO) was obtained from Merck Millipore, Darmstadt, Germany. The cellulose nitrate membrane filters with 0.45 μM pore size were purchased from Whatman GmbH, Dassel, Germany. Polyvinylidene fluoride (PVDF) membrane filters of 0.45 μM pore size were obtained from Merck Millipore, Darmstadt, Germany.

Ultrapure (Type 1) water obtained from the Milli-Q water purification system of Merck Millipore, Darmstadt, Germany.

3.2 Methods

3.2.1 pH measurements

pH measurements of different solutions were made using a delta 320 pH meter (Mettler-Toledo GmbH, Switzerland), attached with a HA405-K2/120 combination electrode. pH meter calibration was made using standard buffers of pH 7.0 and pH 10.0

before the pH measurements in the neutral and alkaline pH ranges, respectively. The least count value of the pH meter was 0.01 pH unit.

3.2.2 Preparation of the stock solutions

The stock solution of HSA was prepared in 60 mM sodium phosphate buffer, pH 7.4. The protein concentration was determined spectrophotometrically using a molar extinction coefficient ($\mathcal{E}_m$) of 36 500 M^{-1} cm^{-1} at 280 nm (Painter et al., 1998). The stock solution was kept at 20 ℃ and used within a week of preparation. The stock solution was diluted with 60 mM sodium phosphate buffer, pH 7.4 to the desired concentration to prepare the working solutions.

The drug (SDN) stock solution was prepared by dissolving 5 mg of its crystals into 5 ml of DMSO. The stock solution was kept at 20 ℃ and was diluted with 60 mM sodium phosphate buffer, pH 7.4 to the desired concentration to prepare the working solutions.

The stock solutions of site markers (WFN, DZM and HMN) were also prepared in DMSO and stored at 20 ℃. The working solutions were made by diluting the stock solutions with 60 mM sodium phosphate buffer, pH 7.4. A value of $\mathcal{E}_m$ = 13, 600 M^{-1} cm^{-1} at 310 nm (Twine et al., 2003) was used to determine the WFN concentration.

Various metal salt solutions were prepared by dissolving their crystals in Milli-Q water. The metal salts used were magnesium chloride ($MgCl_2$), potassium chloride (KCl), calcium chloride ($CaCl_2$), manganese (II) chloride ($MnCl_2$), copper (II) chloride ($CuCl_2$), and barium chloride ($BaCl_2$). The working solutions were prepared by diluting them with water.

3.2.3 Fluorescence spectroscopy

Fluorescence measurements were carried out on a Jasco FP-6500 spectrofluorometer (Jasco International Co., Japan), set up with a 150 W Xenon lamp. A quartz cuvette of

1 cm path length was used by placing it in a thermostatically controlled water-jacketed cell holder, which was connected to a Protech 632D circulating water bath. The widths of the excitation and emission slits were fixed at 10 nm each, while the detector voltage sensitivity was maintained at 240 V. A response time of 2 sec and scan speed of 500 nm min^{-1} was used throughout these studies. The excitation wavelength (λ_{ex}) was fixed at 280 nm while the emission wavelength range was selected from 300 nm to 400 nm.

The three-dimensional (3-D) fluorescence spectra of HSA (3 μM) were obtained in the absence and the presence of SDN with [SDN]:[HSA] molar ratios as 3:1 and 6:1, using the excitation wavelength range from 220–350 nm (5 nm intervals), while the emission wavelength range was fixed from 220–500 nm.

3.2.4 Absorption spectroscopy

Ultraviolet-visible (UV-Vis) absorption measurements were made on Shimadzu UV-2450 UV-Vis spectrophotometer (Shimadzu, Japan), using a pair of 10 mm path length quartz cuvettes. The absorption spectra of HSA (15 μM), SDN-HSA mixtures (1:1, 2:1 and 4:1) and SDN solutions (15, 30 and 60 μM) were obtained by scanning the samples between the wavelengths of 240 nm and 320 nm.

Alternatively, the absorption spectra of the protein (3 μM HSA) and SDN-HSA mixtures with increasing SDN concentrations (3–24 μM with 3 μM intervals) were also acquired in the wavelength range, 300–400 nm. The absorption data, thus obtained were used for the inner filter effect correction of the fluorescence data.

3.2.5 Circular dichroism spectroscopy

Circular dichroism (CD) spectra were obtained on J-815 spectropolarimeter (Jasco International Co., Japan), equipped with a thermostatically controlled water-jacketed cell holder under constant nitrogen flow at 298 K. The far-UV (200–250 nm) CD spectra were

collected using 1 mm path length quartz cuvette and a protein concentration of 3 μM, whereas a 10 mm path length quartz cuvette and 6 μM protein concentration were used to record the near-UV (250–300 nm) CD spectra. The CD spectra were recorded both in the absence and the presence of SDN using the [SDN]:[HSA] molar ratio of 1:1. A data pitch of 1 nm, response time of 0.5 sec and scanning speed of 100 nm min^{-1} were employed to record these spectra at 298 K. The observed CD values (θ_{obs}) were converted to mean residue ellipticity (MRE) values, using Eq. (3.1) (Chen et al., 1972) :

$$\text{MRE} = \frac{\theta obs \times \text{MRW}}{Cp \times l \times 10} \tag{3.1}$$

where MRW refers to the mean residue weight (molecular weight of protein (66, 500 Da) / total number of amino acids (585)), while C_p and l are the concentration of protein in mg ml^{-1} and cuvette length in cm, respectively.

The α-helical content of HSA in the absence and presence of SDN was calculated from the MRE_{208} value using the equation, given below (Lu et al., 1987):

$$\alpha-\text{helix}\ (\%) = \left[\frac{(-\text{MRE}_{208} - 4000)}{33000-4000}\right] \times 100 \tag{3.2}$$

3.2.6 SDN-HSA interaction studies

The interaction studies between SDN and HSA were made using the fluorescence quenching titration method as described below.

3.2.6.1 Fluorescence quenching titration

A constant amount of protein (3 μM HSA) was titrated with SDN using increasing concentrations (3−24 μM with 3 μM intervals) in different tubes, while making the total volume to 6 ml with 60 mM sodium phosphate buffer, pH 7.4. The solution mixture was vortexed prior to incubation for 30 min at the desired temperatures (290, 300, 310 and 313 K). A further incubation of 6 min at the desired temperature was made after placing

the sample-filled cuvette into the cuvette holder. An emission wavelength range of 300−400 nm was used to record the fluorescence intensity using λ_{ex} of 280 nm.

3.2.6.2 Inner filter effect correction

The fluorescence spectral data were corrected for the inner filter effect as suggested by Lakowicz (2006); using the following equation:

$$F_{cor} = F_{obs}\, 10^{(A_{ex}+A_{em})/2} \tag{3.3}$$

where F_{cor} is the corrected fluorescence intensity and F_{obs} is the measured fluorescence intensity. A_{ex} and A_{em} represent the difference in the absorbance values of the protein measured in the presence of ligand at the excitation (λ_{ex}) and emission (λ_{em}) wavelengths, respectively.

3.2.6.3 Fluorescence data analysis

The Stern-Volmer equation was employed to analyse the quenching mechanism involved in SDN-HSA system. The fluorescence data were treated according to the following Stern-Volmer equation (Lakowicz, 2006), as shown below:

$$F_0 / F = K_{SV}\,[Q] + 1 = k_q \tau_0\,[Q] + 1 \tag{3.4}$$

where F_0 and F are the fluorescence intensity values of HSA in the absence and the presence of the quencher (SDN), respectively. K_{SV} is the Stern-Volmer constant and $[Q]$ is the concentration of the quencher.

The bimolecular quenching rate constant (k_q) for SDN-HSA interaction was calculated from the K_{SV} values with the help of Eq. (3.5) using the average lifetime of HSA without quencher (τ_0) as 6.38×10^{-9} sec (Abou-Zied & Al-Shihi, 2008).

$$k_q = K_{SV} / \tau_0 \tag{3.5}$$

The binding constant, K_a values for SDN-HSA system were determined by analysing the fluorescence data using the following double logarithmic equation (Bi et al., 2004):

$$\log (F_0 - F)/ F = \mathrm{n} \log K_a - \mathrm{n} \log [1/ ([L_T - (F_0 - F)[P_T]/ F_0) \quad (3.6)$$

where $[L_T]$ and $[P_T]$ represent the total concentration of the ligand and the protein, respectively.

3.2.6.4 Thermodynamic parameters

The van't Hoff equation was used to determine the thermodynamic parameters; *i.e.,* enthalpy change (ΔH) and entropy change (ΔS) of SDN-HSA interaction.

$$\ln K_a = -\Delta H/RT + \Delta S/ R \quad (3.7)$$

where R is the gas constant (8.314 J mol^{-1} K^{-1}) and T is the absolute temperature (273 +_℃). Values of ΔH and ΔS were obtained from the slope and intercept values of the van't Hoff plot, between ln K_a and 1/T.

The values of the free energy change of the binding reaction (ΔG) at different temperatures were calculated by substituting the values of ΔH and ΔS into the following equation:

$$\Delta G = \Delta H - T\Delta S \quad (3.8)$$

3.2.7 Electrochemical studies

The electrochemical studies on SDN-HSA system were performed on an Auto-142 labPGSTAT30 potentiostat / galvanostat (Ecochemie, Neterlands). The cyclic voltammetry and differential pulse voltammetry were conducted in a compartment of 10 ml single three-electrode glass cell containing Ag/AgCl as the reference electrode, platinum wire as the counter electrode and glassy carbon electrode (GCE) of 3 mm diameter as the working electrode. GCE was polished gently with 0.3 micron Al_2O_3 slurry

on a polishing cloth, followed by rinsing with distilled water before each experiment. All measurements were performed at 298 K. The cyclic voltammetry was performed using 3 μM HSA, 48 μM SDN and 9SDN-HSA (6:1) mixture in 60 mM sodium phosphate buffer, pH 7.4, pre-incubated for 30 min at 298 K and scanning them in the potential range, 0.5–1.0 V with the scan speed of 0.1 V.

The differential pulse voltammetry was further performed for quantitative determination of SDN on HSA using 3 μM HSA, while varying the SDN concentration as 0, 18, 24, 30, 36, 42 and 48 μM. The mixtures were stirred for 10 sec before current measurement in the potential range, 0.75–0.90 V with the scan speed of 0.1 V.

3.2.8 Thermal stability studies

Thermal stability of the protein was assessed in the absence and presence of SDN by recording fluorescence intensity at 342 nm within the temperature range of 303–343 K. The samples contained either 3 μM HSA or SDN-HSA (6:1) mixture, pre-incubated for 30 min at 298 K. These samples were further incubated for 8 min at each temperature within the studied range, before fluorescence intensity measurements.

3.2.9 Identification of the SDN binding site

The SDN binding site identification on HSA was made by carrying out the competitive ligand-displacement as well as molecular docking studies.

3.2.9.1 Competitive ligand-displacement studies

Three site markers, *viz*., WFN for Site I, DZM for Site II and HMN for Site III were used in competitive ligand-displacement experiments. Site marker-HSA (1:1; 3 μM each) mixtures were pre-incubated at 298 K for 30 min before titrating them with increasing SDN concentrations (3–24 μM; 3 μM intervals) in a total amount of 6 ml. The solution mixtures were vortexed and further incubated for 30 min at 298 K. The fluorescence

spectra of mixtures containing WFN were recorded in the wavelength range, 360–480 nm using λ_{ex} of 335 nm. On the other hand, DZM and HMN containing mixtures were analysed for fluorescence intensity measurements at 342 nm using λ_{ex} of 280 nm. Parallel experiments with 3 μM HSA without site marker were also carried out under similar conditions to act as a control.

3.2.9.2 Molecular docking studies

The three-dimensional (3-D) structure of HSA [PDB ID:1BM0] was selected from the Protein Data Bank while the 3-D structure of SDN was generated with Avogadro software (Hanwell et al., 2012) and further amended using the MMFF94 force field (Halgren, 1996). The PDB ID: 1BM0 entry was chosen for this docking study since it is in apo-form (no bounded ligand), with no missing residues, absence of any form of mutation and within a relatively good resolution limit (2.50 Å). Moreover, other studies have also used this structure in their projects (Hu et al., 2011; Sharifi & Ghayeb, 2018). Prior to molecular docking, removal of crystallized water molecules, addition of non-polar hydrogens and computation of Kollman charges were performed for HSA structure using AutoDockTools 4 (Morris et al., 2009). Independent docking for both of the Sudlow's binding sites on HSA (Sudlow et al., 1975) was conducted by specifying the grid box as x: 35.35, y: 32.41, z: 36.46 for Site I and x: 14.42, y: 23.55, z: 23.31 for Site II on HSA with the dimension of 70 × 70 × 70 grid points. The molecular docking with AutoDock4 (Morris et al., 2009) was executed by selecting Lamarckian genetic algorithm as the search engine with the parameters set to 100 search runs, 150 population size, while the generation and energy evaluation were fixed to 27,000 and 250,000, respectively. Analysis of the docking simulation was done by using the root-mean-square deviation (RMSD) of 2.0 Å in clustering the obtained results. The interaction generated by the complex was visualized and captured using UCSF Chimera (Pettersen et al., 2004).

LigPlot+ was used in observing the interaction of SDN with the binding Site I of HSA (Wallace et al., 1995).

3.2.10 Influence of metal ions on SDN-HSA interaction

To study the effect of metal ions on SDN-HSA interaction, a fixed amount of metal salts was added to the protein solution followed by incubation for 1 hour at 298 K. The titrations of HSA in the presence of increasing concentrations of SDN (3–24 μM) were performed in the same way as described in Section 3.2.6.1. The final concentrations of HSA and metal salts ($MgCl_2$, KCl, $CaCl_2$, $MnCl_2$, $CuCl_2$ and $BaCl_2$) were 3 μM and 30 μM, respectively. An additional incubation time of 30 min was used after the addition of SDN before fluorescence measurements (Kabir et al., 2017). Analysis of the fluorescence data were made in the same way as described earlier (Section 3.2.6.3) to determine the K_a values.

3.2.11 Statistical analysis

All experiments were conducted at least three times and the results are reported as the average values with the mean standard deviation. The processing, curve fitting and smoothing of the curves were employed using the OriginPro 8.5 software (OriginLab Corp., Northampton, Massachusetts, US

CHAPTER 4: RESULTS AND DISCUSSION

4.1 SDN-HSA interaction

Fluorescence spectroscopy is a widely used technique in studying ligand-protein interaction due to its high sensitivity to local environmental change, rapid measurement and simple quantitative analysis (Brand & Johnson, 2008; Oravcova et al., 1996; Valeur, 2009). Fluorescence detection in proteins is employed in exploring the change around the fluorophore's microenvironment upon ligand binding, which subsequently produces reliable information about ligand-protein interaction (Mocz & Ross, 2013; Sharma & Schulman, 1999). The fluorescence characteristics of HSA are due to the presence of aromatic amino acid residues*, i.e.,* tryptophan (Trp), tyrosine (Tyr) and phenylalanine (Phe). However, the intrinsic fluorescence of the protein is mainly contributed by sole tryptophan (Trp-214) residue as the Tyr fluorescence is usually quenched in its ionized form or due to the presence of neighbouring amino groups, carboxyl groups or Trp residue, while quantum yield of Phe is very low (Chen & Barkley, 1998; Möller & Denicola, 2002). Therefore, interaction of SDN with HSA was studied by employing the fluorescence quenching titration method.

4.1.1 Fluorescence quenching titration results

All fluorescence spectra of HSA and SDN-HSA mixtures were corrected for the inner filter effect as described in Section 3.2.6.2. Figure 4.1 (A–D) displays the corrected fluorescence spectra of HSA in the wavelength range between 300 nm and 400 nm, obtained in the absence and the presence of increasing concentrations of SDN at 290 K, 300 K, 310 K and 313 K, respectively, when excited at 280 nm. The advent of the emission maxima at 342 nm was reflective of the presence of Trp in HSA (Lakowicz, 2006). A progressive decrease in the fluorescence intensity (fluorescence quenching) of HSA at 342 nm was observed upon concurrent addition of increasing concentrations of

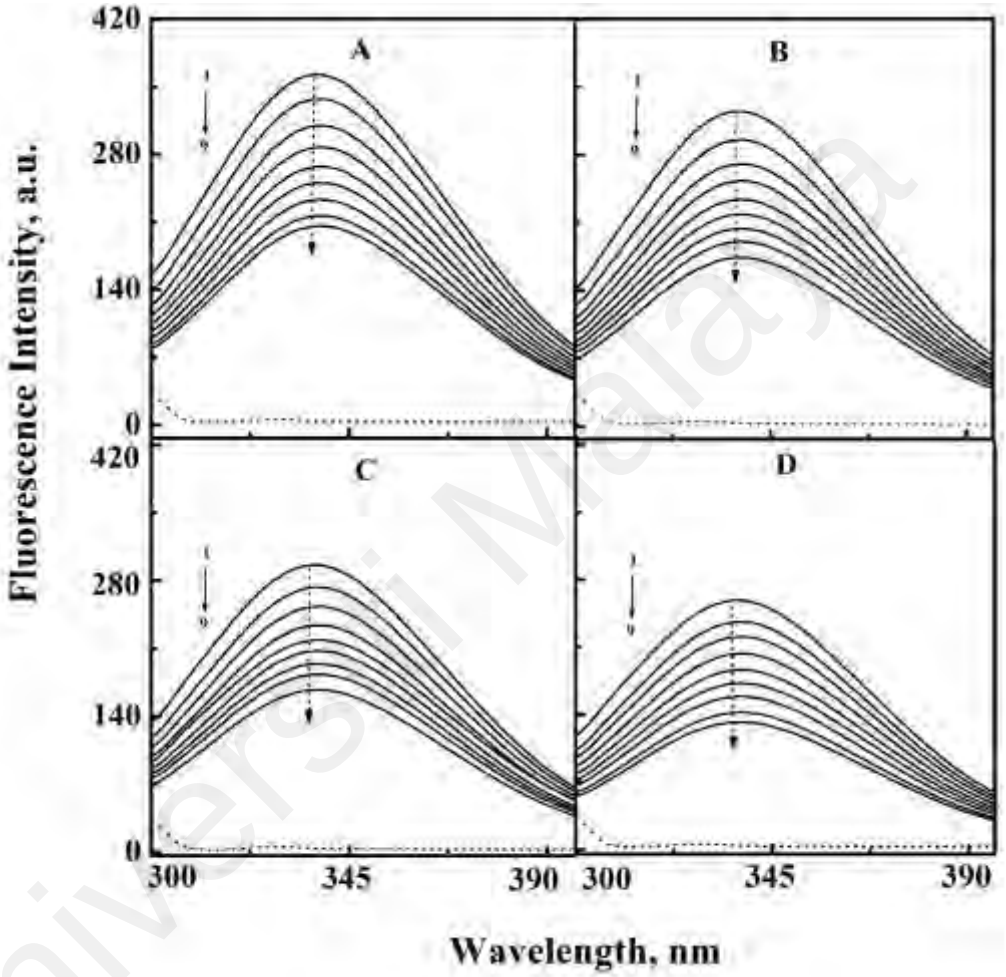

Figure 4.1: Fluorescence spectra of HSA in the absence and the presence of increasing SDN concentrations at four different temperatures, *i.e.,* 290 K (A), 300 K (B), 310 K (C) and 313 K (D), obtained in 60 mM sodium phosphate buffer, pH 7.4, upon excitation at 280 nm. The concentration of HSA was 3 µM while the concentration of SDN (from top to bottom, 1→9) varied as 0–24 µM with regular increments of 3 µM. Fluorescence spectrum of free SDN (24 µM) is represented by dotted lines.

SDN at all the studied temperatures. However, the decrease was found to be inversely correlated with temperature *i.e.,* the decrease became lesser with increasing temperature at all SDN concentrations (Figure 4.2). The highest SDN concentration (24 μM) produced a pronounced decrease in the fluorescence intensity along with significant blue shift in the emission maxima. Values of the percentage decrease in the fluorescence intensity along with the extent of blue shift in the emission maxima, observed at different temperatures were ~ 48 %, 3 nm (290 K); ~ 46 %, 4 nm (300 K); ~ 41%, 3 nm (310 K) and ~ 37 %, 3 nm (313 K), respectively. The blue shift could be due to the change in the microenvironment (from polar to nonpolar) around Trp-214 residue of the protein (Brodersen et al., 1977). It may be noted that free SDN did not show any significant fluorescence intensity within this wavelength range (spectra shown as dotted lines in Figure 4.1).

4.1.2 Mechanism of quenching

The fluorescence quenching can be classified as static or dynamic quenching, which can be distinguished based on time-resolved fluorescence decay as well as temperature dependence (Lakowicz, 2006). In order to characterize the SDN-induced quenching, SDN-HSA titration results, obtained at four different temperatures (290, 300, 310 and 313 K) were analysed according to Eq. (3.4). The Stern-Volmer plots shown in Figure 4.3 was found linear in the concentration range used, suggesting involvement of a single quenching mechanism. The values of the Stern-Volmer constant (K_{SV}) were obtained from the slopes of the linear Stern-Volmer plots (Figure 4.3) and are given in Table 4.1. Our results showed increase in the K_{SV} value with increasing temperature, thus characterizing the SDN-induced quenching of protein fluorescence as dynamic quenching. In order to adjudicate the SDN-induced quenching of HSA fluorescence, we calculated the value of the bimolecular quenching rate constant, k_q of SDN-HSA system at four different temperatures, using Eq. (3.5). Interestingly, the k_q values (Table 4.1) were

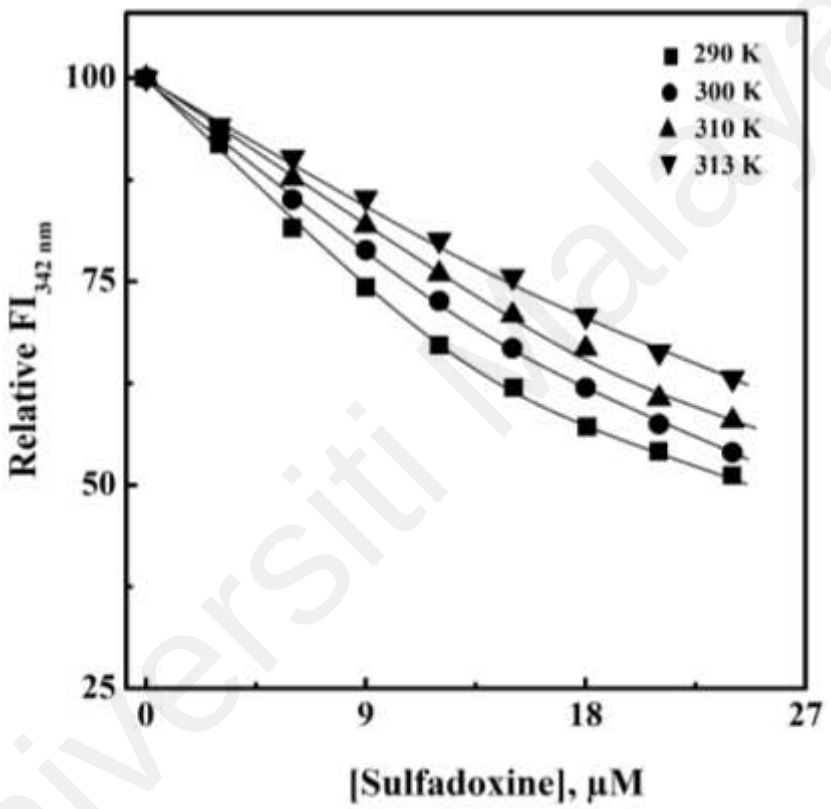

Figure 4.2: Plot showing the decrease in the relative fluorescence intensity at 342 nm (Relative $FI_{342\ nm}$) of HSA with increasing concentrations of SDN at four different temperatures, *i.e.,* 290 K, 300 K, 310 K and 313 K. Values of the $FI_{342\ nm}$ at different SDN concentrations were taken from the data, shown in Figure 4.1.

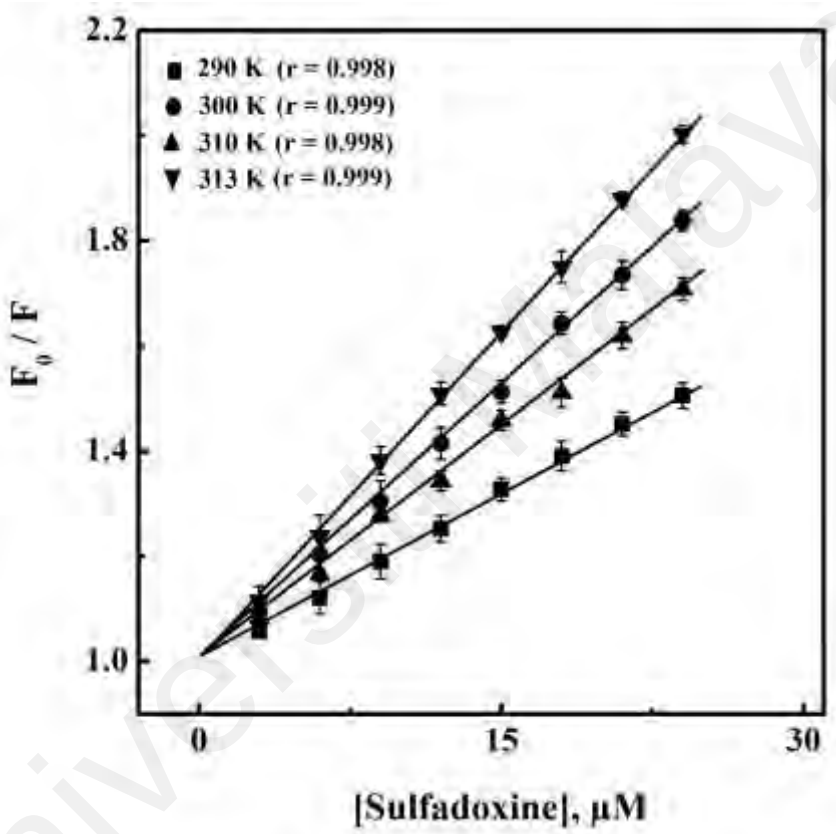

Figure 4.3: Stern-Volmer plots for the fluorescence quenching data of the SDN-HSA system, obtained in 60 mM sodium phosphate buffer, pH 7.4 at four different temperatures, *i.e.,* 290 K, 300 K, 310 K and 313 K.

Table 4.1: Values of the quenching constant, bimolecular quenching rate constant, binding constant and thermodynamic parameters of SDN-HSA binding reaction at four different temperatures.

T (K)	$K_{SV} \times 10^4$ (M^{-1})	$k_q \times 10^{12}$ ($M^{-1}\,s^{-1}$)	$K_a \times 10^4$ (M^{-1})	n	ΔS (J $mol^{-1}\,K^{-1}$)	ΔH (kJ mol^{-1})	ΔG (kJ mol^{-1})
290	3.15±0.04	4.94	3.22±0.01	0.98±0.00			– 25.03
300	3.39±0.01	5.31	3.49±0.02	0.99±0.01	+ 104.42	+ 5.25	– 26.07
310	3.51±0.03	5.50	3.58±0.08	1.00±0.01			– 27.12
313	3.81±0.06	5.97	3.88±0.07	0.98±0.01			–27.43

found higher than the maximum dynamic quenching rate constant ($2.0 \times 10^{10}\ M^{-1}s^{-1}$), thus supported SDN-induced quenching of protein fluorescence as static quenching.

To further confirm the static quenching, involved in the SDN-HSA system and complex formation between SDN and HSA, UV-Vis absorption spectra of HSA were recorded in the absence and the presence of increasing SDN concentrations. The excited state of the fluorophore will only be affected in dynamic quenching without changing the UV-Vis absorption spectrum, while significant changes occur in the UV-Vis absorption spectrum due to ground state complex formation in static quenching. As can be seen from Figure 4.5, the UV-Vis absorption spectrum of HSA was significantly affected upon addition of SDN, which suggested complex formation between SDN and HSA. The UV-Vis absorption spectra of HSA in the presence of SDN, as shown in Figure 4.5 were obtained after subtracting the UV-Vis absorption spectra of free SDN (Figure 4.4B) from the UV-Vis absorption spectra of SDN-HSA mixtures (Figure 4.4 A). Therefore, these results strongly suggested the involvement of static quenching mechanism and thus complex formation between SDN and HSA.

4.1.3 Binding constant

The fluorescence quenching titration data obtained at four different temperatures were transformed into double logarithmic plots (Figure 4.6) using Eq. (3.6), which were used to determine the binding constant (K_a) for SDN-HSA interaction. The K_a values thus obtained are shown in Table 4.1. These values were noticed to fall in the order of 10^4, which implied a moderate binding affinity between SDN and HSA. Such binding affinity is beneficial for the drug transport via blood circulation, as it may favour the optimum distribution and its easy release at the target site. This may also increase the drug's efficacy and enhance its therapeutic effects at the target site (Chaves et al., 2015). Many published reports have shown the binding affinity between the transport protein and the

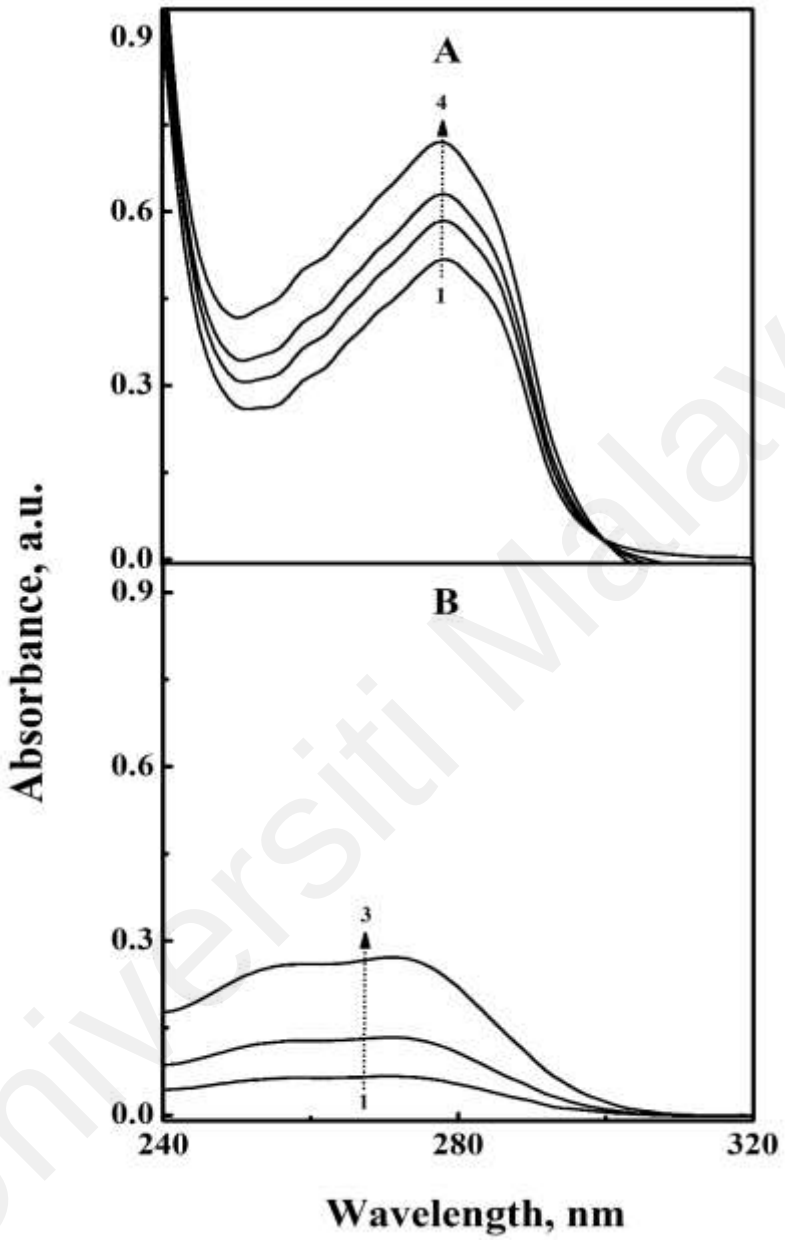

Figure 4.4: (A). UV-Vis absorption spectra of 15 µM HSA (spectrum '1') and SDN-HSA mixtures *i.e.,* 1:1 (spectrum '2'), 2:1 (spectrum '3') and 4:1 (spectrum '4'). (B). UV-Vis absorption spectra of SDN at 15 µM (spectrum '1'), 30 µM (spectrum '2') and 60 µM (spectrum '3') concentrations. These spectra were obtained in 60 mM sodium phosphate buffer, pH 7.4 at 300 K.

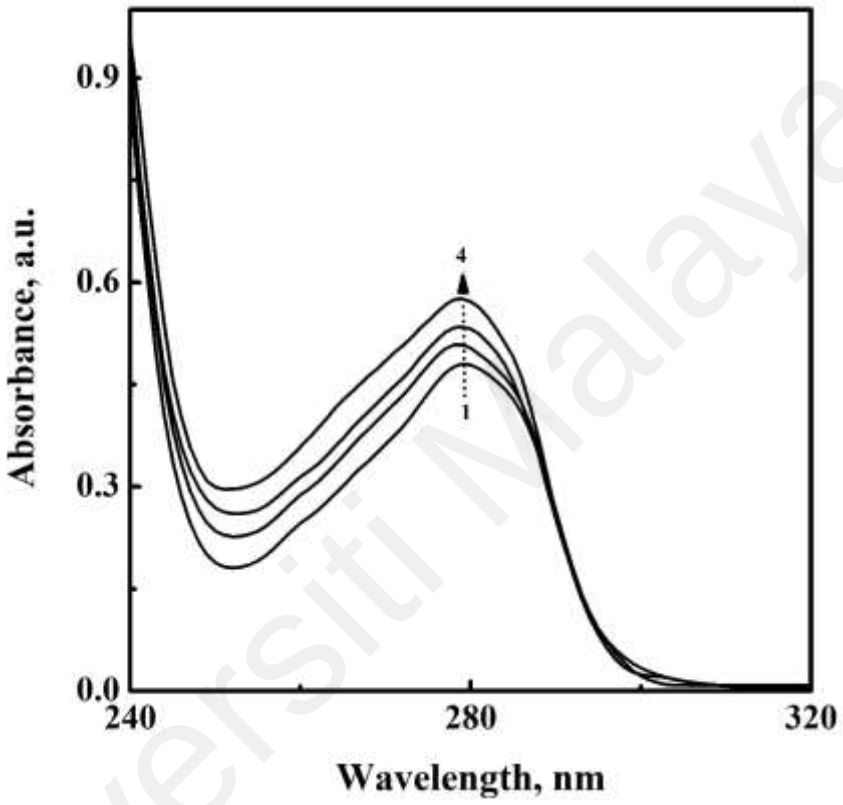

Figure 4.5: UV-Vis absorption spectra of HSA in the absence and the presence of increasing SDN concentrations, obtained in 60 mM sodium phosphate buffer, pH 7.4 at 300 K. The concentration of HSA was fixed at 15 µM (spectrum 1) while the concentration of SDN (from bottom to top, 2→4) varied as 15 µM, 30 µM and 60 µM, respectively. These spectra were obtained after subtracting the absorption spectra of SDN (Figure 4.4 (B)) from the absorption spectra of SDN-HSA mixtures (Figure 4.4 (A)).

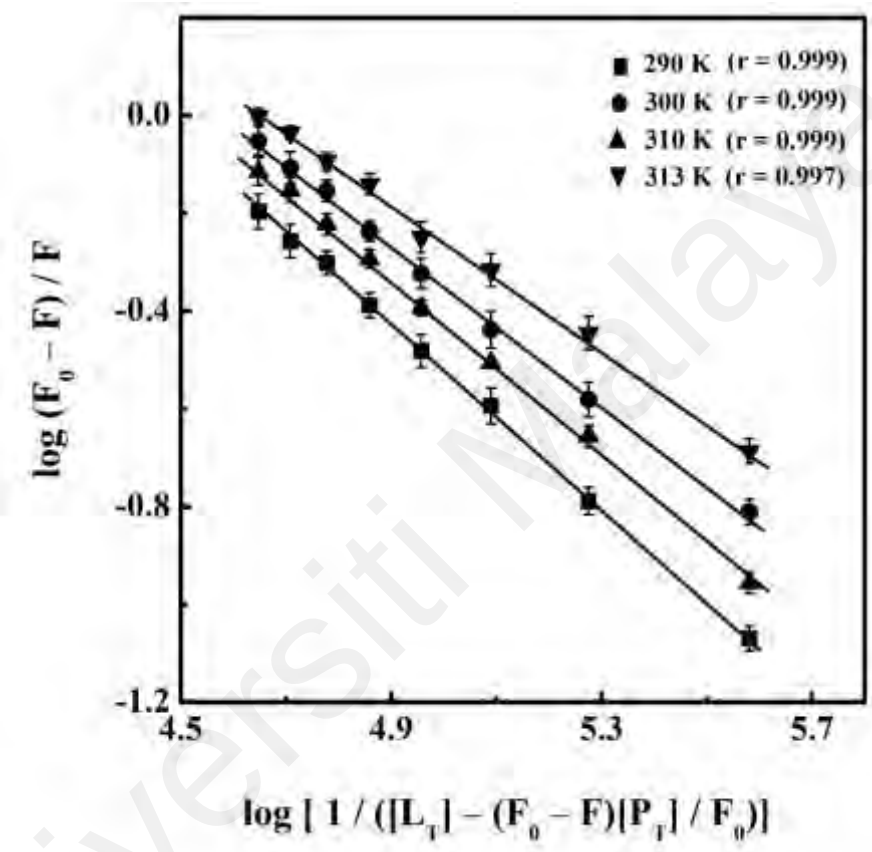

Figure 4.6: Double logarithmic plots of log ($F_0 - F$) / F against log [1 / ([L_T] – (F_0 – F) [P_T] / F_0)] for the fluorescence quenching data of the SDN-HSA system, obtained in 60 mM sodium phosphate buffer, pH 7.4 at four different temperatures, *i.e.,* 290 K, 300 K, 310 K and 313 K.

drugs as moderate (Chadha et al., 2020; Chaves et al., 2018; Mousavi & Fatemi, 2019; Peng et al., 2016; Rastegari et al., 2016). Such range of the binding constant between drugs and HSA, is helpful in altering drugs' distribution and efficacy in human circulation (Keen, 1971; Ranjbar et al., 2013; Zhivkova, 2015) as well as their pharmacokinetics (Keen, 1971). Several published reports have suggested the importance of drug-protein interaction study in understanding the pharmacokinetic criteria of the drugs, which may be useful in the clinical therapy (Liu et al., 2017; Ranjbar et al., 2013; Otagiri, 2005; Yeggoni et al., 2017). Furthermore, K_a value was found to increase with increasing temperature (Table 4.1), which predicted participation of endothermic nonpolar forces in SDN-HSA complex formation, as these forces are strengthened at higher temperatures (Bijari et al., 2013). Values of '*n*' were found to be close to 1.0 (Table 4.1), suggesting single class of SDN binding site on HSA.

4.1.4 Binding forces

In order to confirm the binding forces involved in SDN-HSA interaction, thermodynamic parameters, *i.e.,* enthalpy change (ΔH) and entropy change (ΔS) of the binding reaction were determined, using van't Hoff plot (Figure 4.7). Additionally, values of the Gibbs free energy change (ΔG) were retrieved by substituting the values of ΔS and ΔH into Eq. (3.8). These values of ΔS, ΔH and ΔG are also included in Table 4.1. The negative sign of ΔG revealed spontaneous reaction between SDN and HSA at all temperatures. Positive value of ΔH suggested the interaction as an endothermic reaction. This justified the increase in the K_a values with increase in temperature, as found for SDN-HSA system (Table 4.1). A larger negative value of $T\Delta S$, contributed by positive value of ΔS surmounted the negative contribution of positive ΔH value in making the ΔG negative, thus promoting the feasibility of the reaction. Disruption of the ordered water layers around SDN and HSA molecules, when SDN-HSA complex is formed, was responsible for increasing the entropy. According to Ross & Subramanian (1981), binding force

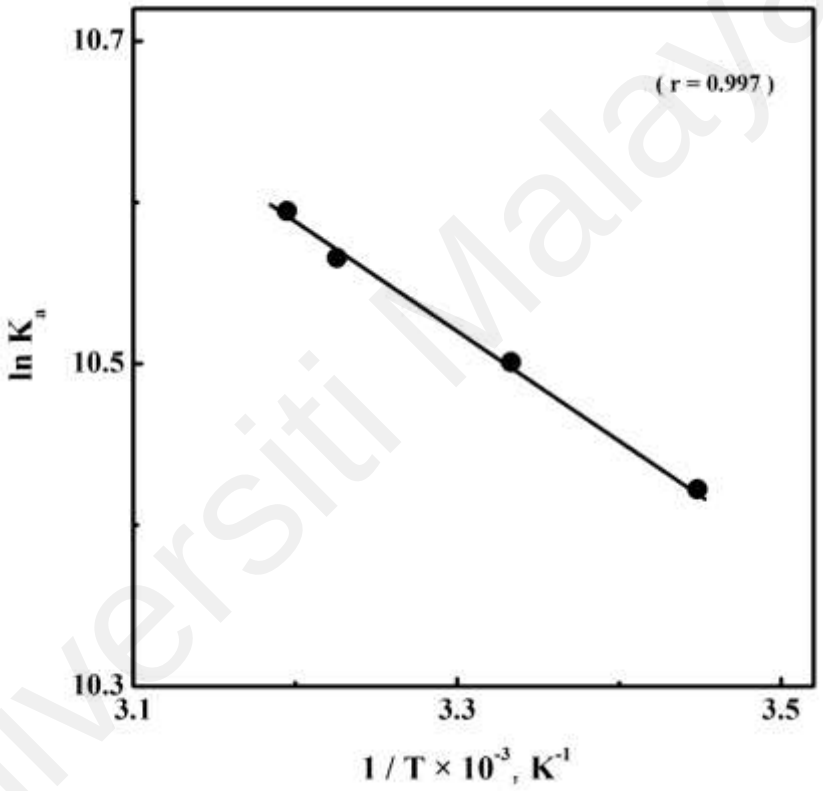

Figure 4.7: The van't Hoff plot for the interaction between SDN and HSA.

involved in ligand-protein complex formation can be predicted as hydrophobic force if both ΔS and ΔH values are positive. In view of it, SDN-HSA interaction seems to be stabilised primarily by hydrophobic interactions. However, other forces such as hydrogen bonds, as deduced from molecular docking results (Section 4.1.9.2) might have added to the stability of SDN-HSA complex.

4.1.5 SDN-induced electrochemical changes in HSA

Cyclic voltammetry has also been exploited to show complex formation between protein and small molecules (Magdum et al., 2017; Maurya et al., 2019; Wu et al., 2019). In view of it, variations in the electrochemical signals were monitored to investigate the interaction between HSA and SDN at pH 7.4. No significant electrochemical response was noticed from free HSA or SDN solutions. Nevertheless, SDN-HSA mixture produced a visible oxidation peak to a slightly higher potential (0.82 V) with an increase in the oxidation current (1.52 μA) (Figure 4.8). Such current change was suggestive of the formation of SDN-HSA complex. To support this idea, interaction of SDN with HSA was studied by monitoring the increase in the peak current from the differential pulse voltammograms (Figure 4.9), using increasing concentrations of SDN and fixed concentration of HSA. A linear relationship between the peak current and SDN concentration was observed (Figure 4.10), suggesting complex formation between SDN and HSA. This can be explained due to the presence of more intercalation sites for binding to HSA. Thus, the voltammetric results supported the spectroscopic observations for SDN-HSA complex formation.

4.1.6 SDN-induced secondary and tertiary structural changes in HSA

CD spectra in the far-UV and the near-UV regions provide useful information about protein's secondary and tertiary structures as well as alterations in them, if any, upon ligand addition (Greenfield, 2006; Kelly & Price, 1997). The far-UV and the near-UV

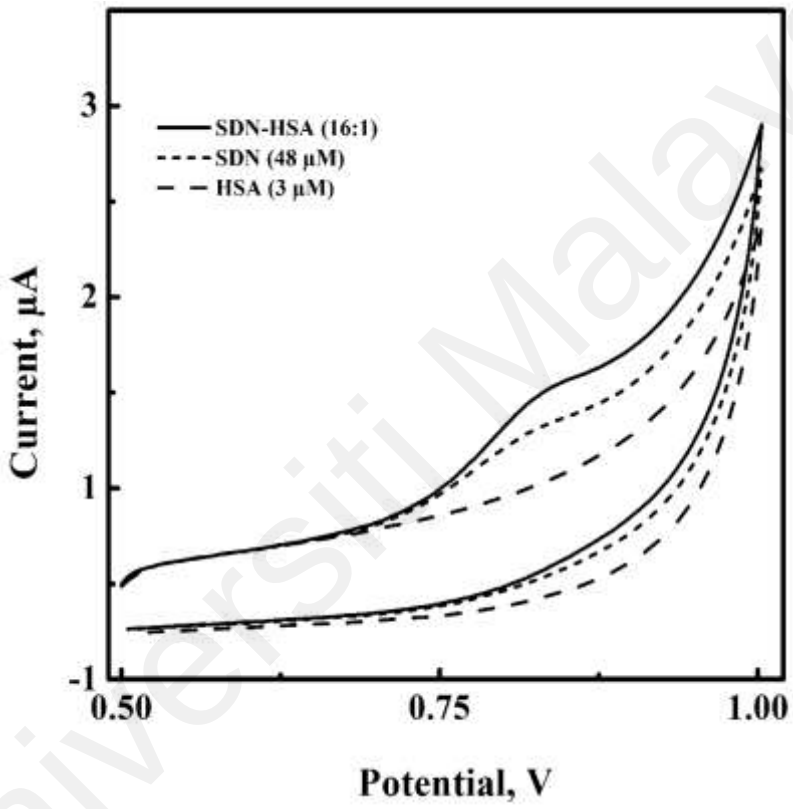

Figure 4.8: Cyclic voltammograms of HSA, SDN and SDN-HSA mixture, obtained in 60 mM sodium phosphate buffer, pH 7.4 in the potential range of 0.5–1.0 V, using the scan speed of 0.1 V. The concentrations of HSA and SDN were 3 µM and 48 µM, respectively.

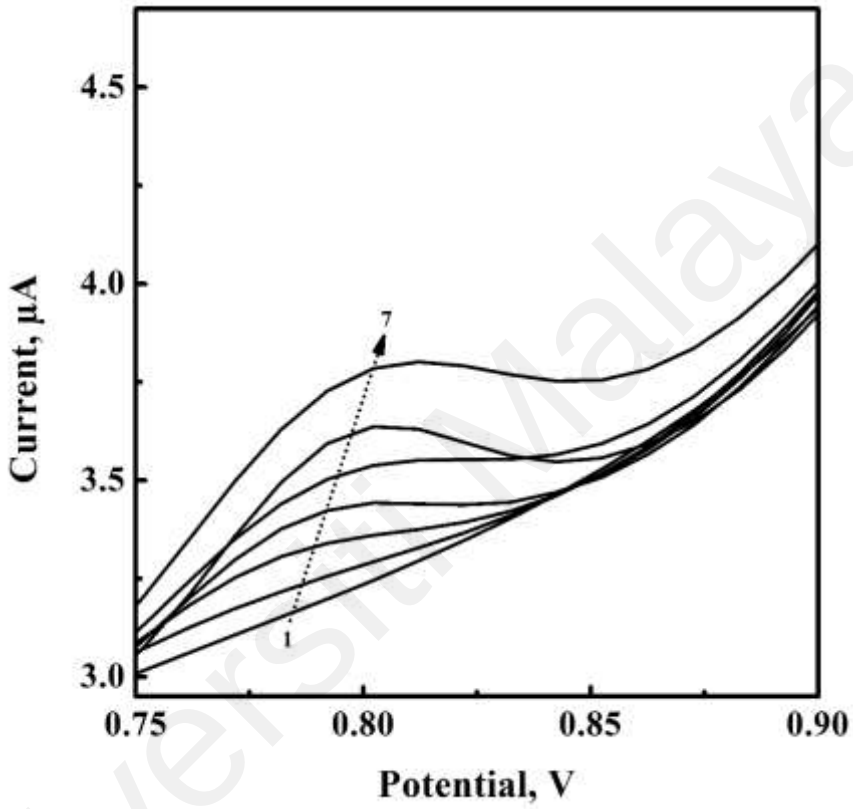

Figure 4.9: Differential pulse voltammograms of HSA in the absence (1) and with increasing concentrations of SDN (2-7), obtained in 60 mM sodium phosphate buffer, pH 7.4 in the potential range of 0.75–0.90 V, using the scan speed of 0.1 V. The concentration of HSA was fixed at 3 µM while the concentration of SDN (2-7) varied as 18 µM, 24 µM, 30 µM, 36 µM, 42 µM and 48 µM, respectively.

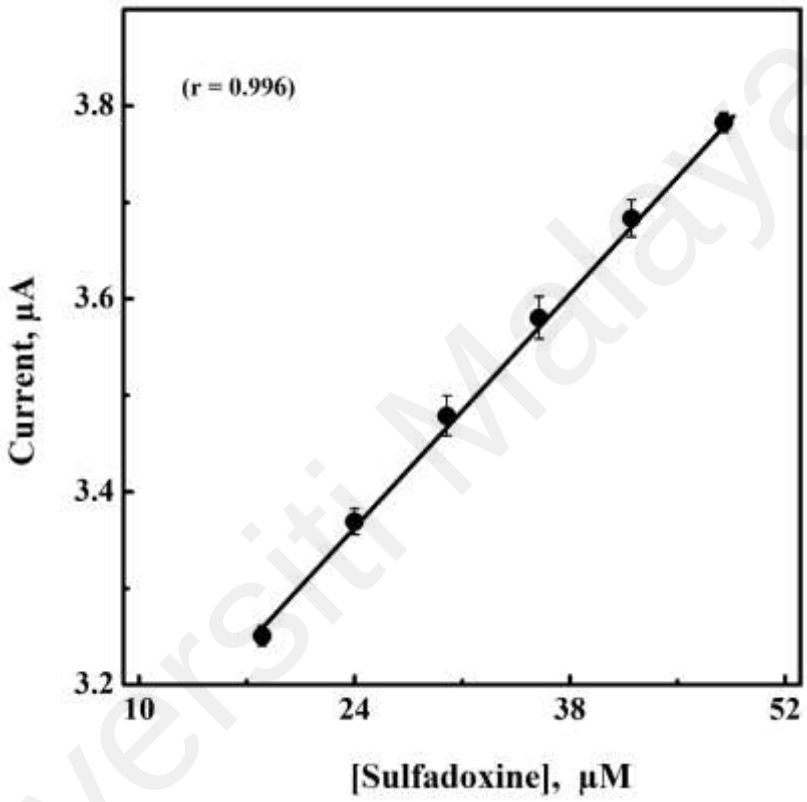

Figure 4.10: Linear plot showing correlation between the peak current in the differential pulse voltammograms of HSA and SDN concentration (Figure 4.9).

CD spectra of HSA and its equimolar (1:1) mixture with SDN are shown in Figure 4.11 and Figure 4.12, respectively. The helical nature of HSA was evident from the appearance of two negative bands at 208 and 222 nm in the far-UV CD spectrum (Figure 4.11). A slight increase in the CD spectral signals at these wavelengths was noticed upon SDN addition (Figure 4.11), which suggested small secondary structural change in the protein. Quantitatively, the α-helical content was increased from 59.7 % to 64.5 % in presence of SDN. Such difference suggested changes in the hydrogen bonding pattern in HSA upon binding of SDN.

The near-UV CD spectra of HSA (Figure 4.12) showed two minima around 261 nm and 268 nm, reflecting presence the aromatic chromophores (Trp and Tyr residues) and disulphide bonds in the protein (Kelly et al., 2005). Presence of SDN produced decrease in the MRE values at these wavelengths, suggesting alteration in the protein's tertiary structure upon SDN addition. Similar changes in the CD spectrum have been demonstrated in many ligand-binding studies (Kabir et al., 2016; Musa et al., 2020; Peng et al., 2014; Wu et al., 2018).

4.1.7 SDN-induced microenvironmental changes in HSA

Advantage of the three-dimensional (3-D) fluorescence spectra was taken to observe microenvironmental changes around protein fluorophores, that occurred upon SDN addition. Figures 4.13–4.15 represent the 3-D fluorescence spectra and corresponding contour maps of HSA and SDN-HSA mixtures in [SDN]:[HSA] molar ratios of 3:1 and 6:1, respectively. The 3-D fluorescence spectra were characterized by the emergence of two pairs of spectral peaks. While peaks 'a' and 'b' were originated due to scattering, peaks '1' and '2' represented fluorescence contribution of Tyr and Trp residues of the protein (Makarska-Bialokoz & Lipke, 2019; Tayyab et al., 2019). Table 4.2 shows position and intensity of these peaks in HSA and SDN-HSA mixtures. Significant

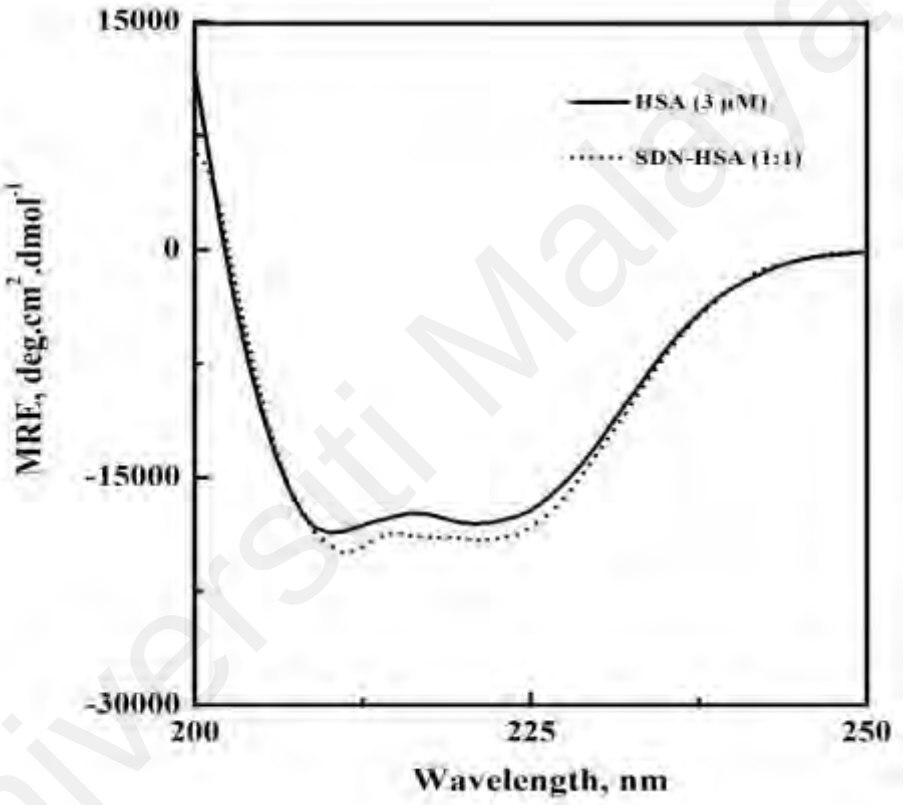

Figure 4.11: Far-UV CD spectra of HSA and SDN-HSA (1:1) mixture. The CD spectra were recorded using a protein concentration of 3 μM in 60 mM sodium phosphate buffer, pH 7.4 at 298 K.

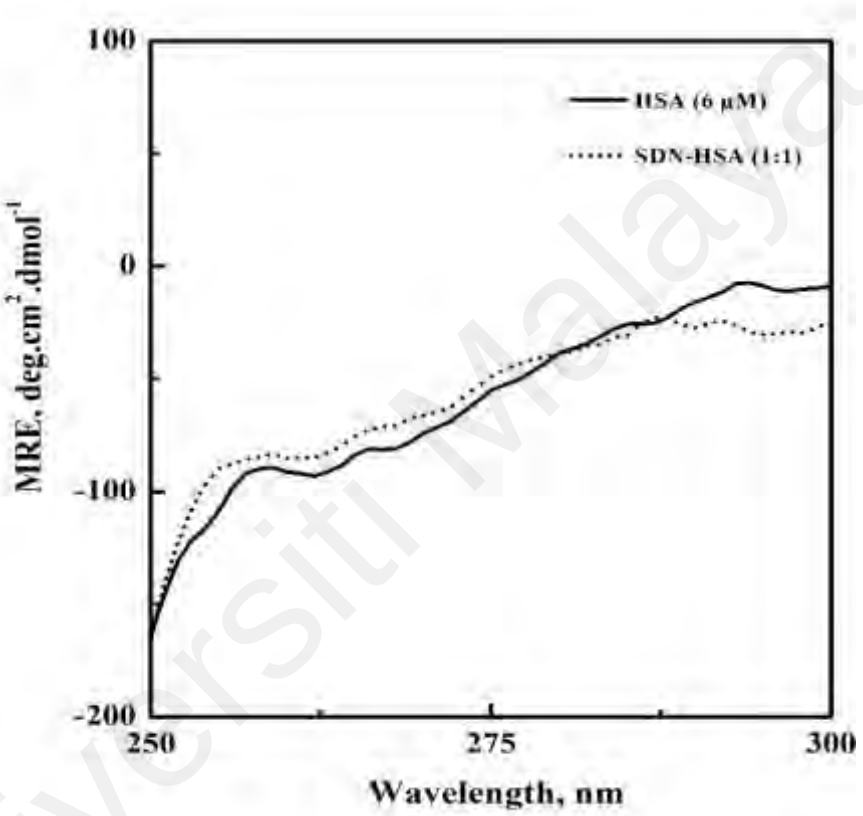

Figure 4.12: Near-UV CD spectra of HSA and SDN-HSA (1:1) mixture. The CD spectra were recorded using a protein concentration of 6 μM in 60 mM sodium phosphate buffer, pH 7.4 at 298 K.

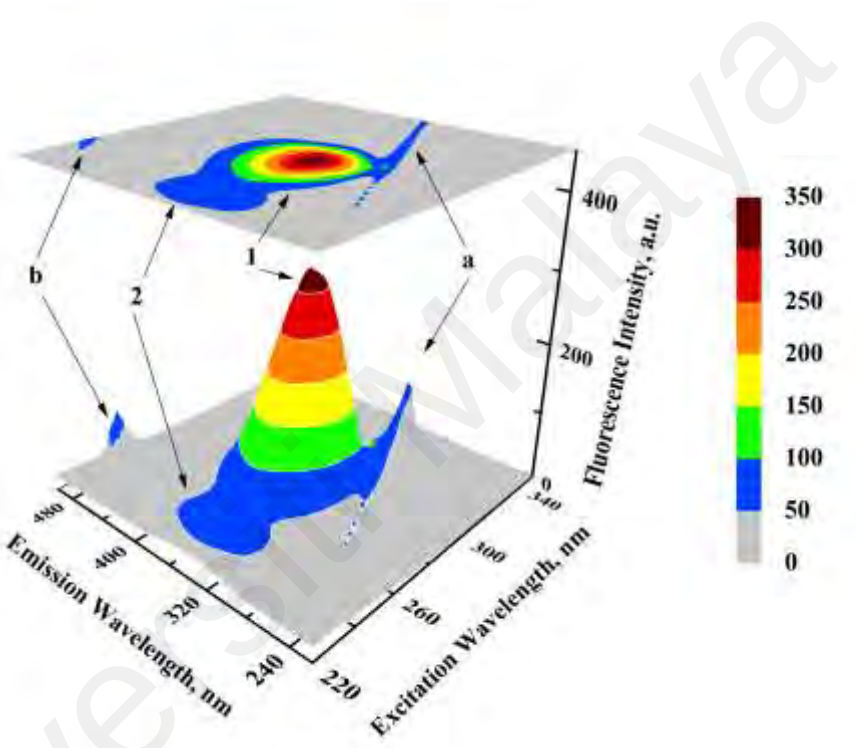

Figure 4.13: Three-dimensional fluorescence spectra and corresponding contour map of 3 µM HSA, obtained in 60 mM sodium phosphate buffer, pH 7.4 at 298 K.

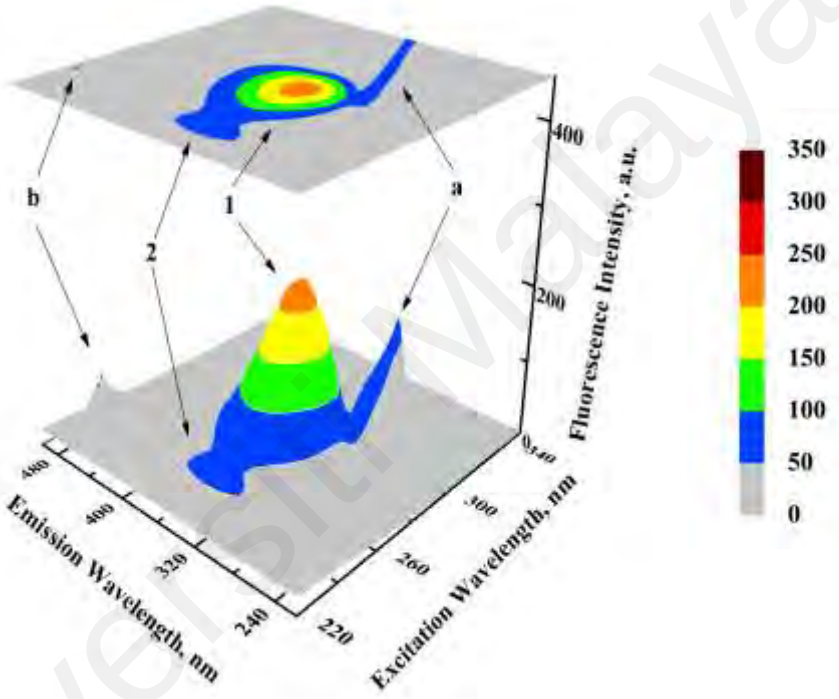

Figure 4.14: Three-dimensional fluorescence spectra and corresponding contour map of SDN-HSA (3:1) mixture, obtained in 60 mM sodium phosphate buffer, pH 7.4 at 298 K. The protein and SDN concentrations were 3 µM and 9 µM, respectively.

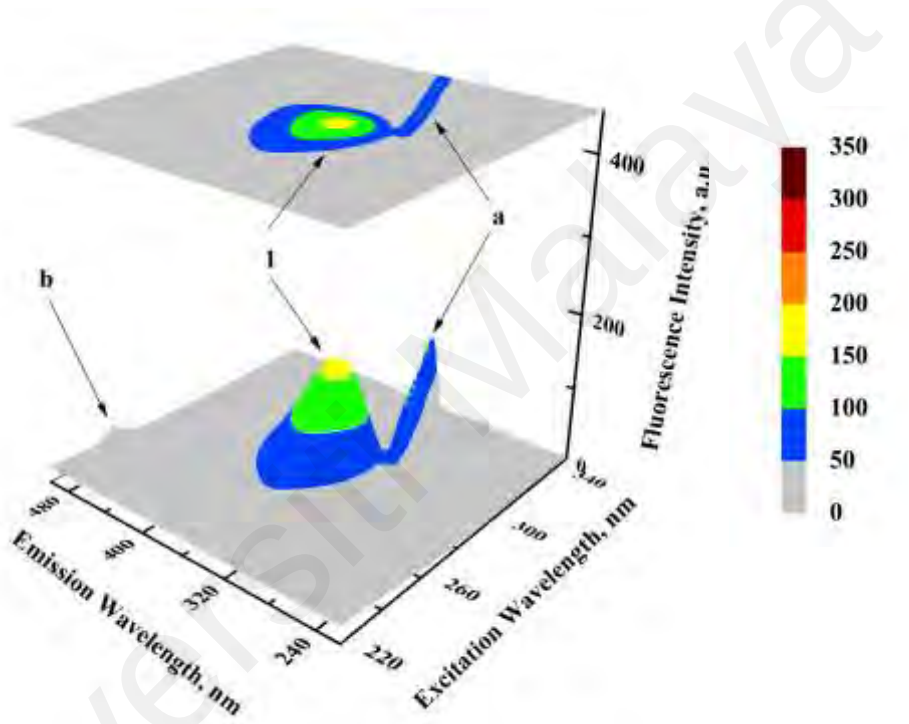

Figure 4.15: Three-dimensional fluorescence spectra and corresponding contour map of SDN-HSA (6:1) mixture, obtained in 60 mM sodium phosphate buffer, pH 7.4 at 298 K. The protein and SDN concentrations were 3 µM and 18 µM, respectively.

Table 4.2: Three-dimensional fluorescence spectral characteristics of HSA and SDN-HSA mixtures, obtained at 60 mM sodium phosphate buffer, pH 7.4.

System	Peak	Peak position [$\lambda_{ex}/\lambda_{em}$, nm/nm]	Intensity
HSA	a	230/230→350/350	22.4→82.1
	b	250/500	71.6
	1	280/338	273.4
	2	230/334	82.2
[SDN]: [HSA] = 3:1	a	230/230→350/350	21.3→89.4
	b	250/500	51.4
	1	280/338	213.1
	2	230/332	43.8
[SDN]: [HSA] = 6:1	a	230/230→350/350	20.1→104.8
	b	250/500	31.8
	1	280/338	138.3
	2	230/333	28.8

reduction in the intensities of peaks '1' and '2' were noticed upon SDN addition. The decrease was ~ 22 % (peak '1') and ~ 47 % (peak '2') at 3:1 [SDN]:[HSA] molar ratio, which increased to ~ 49 % (peak '1') and ~ 64 % (peak '2') at 6:1 [SDN]:[HSA] molar ratio (Table 4.2). Such decrease in the intensity reflected microenvironmental changes around Tyr and Trp residues in the presence of SDN, thus suggesting complex formation between SDN and HSA.

4.1.8 SDN-induced thermal stabilization of HSA

Thermal stability of a protein may be affected in the presence of a ligand, which suggests complex formation between the protein and its ligand (Celej et al., 2003; Shrake & Ross, 1988). Temperature-induced changes in the fluorescence intensity at 342 nm ($FI_{342\ nm}$) of the protein alone as well as ligand-protein (6:1) mixture can be seen from Figure 4.16. The fluorescence intensity decreased progressively with the increase in temperature. However, the decrease was significantly lesser in SDN-HSA mixture compared to the protein alone. Quantitative analysis showed ~ 55% decrease in FI_{342nm} at 343 K with protein alone while only ~ 35 % decrease was observed with SDN-HSA mixture at the same temperature. This suggested increased thermal stability of the protein in presence of SDN as more energy is needed to break additional forces involved in SDN-HSA complex formation.

4.1.9 SDN binding site in HSA

In order to identify the SDN binding site in HSA, both ligand displacement and molecular docking experiments were performed.

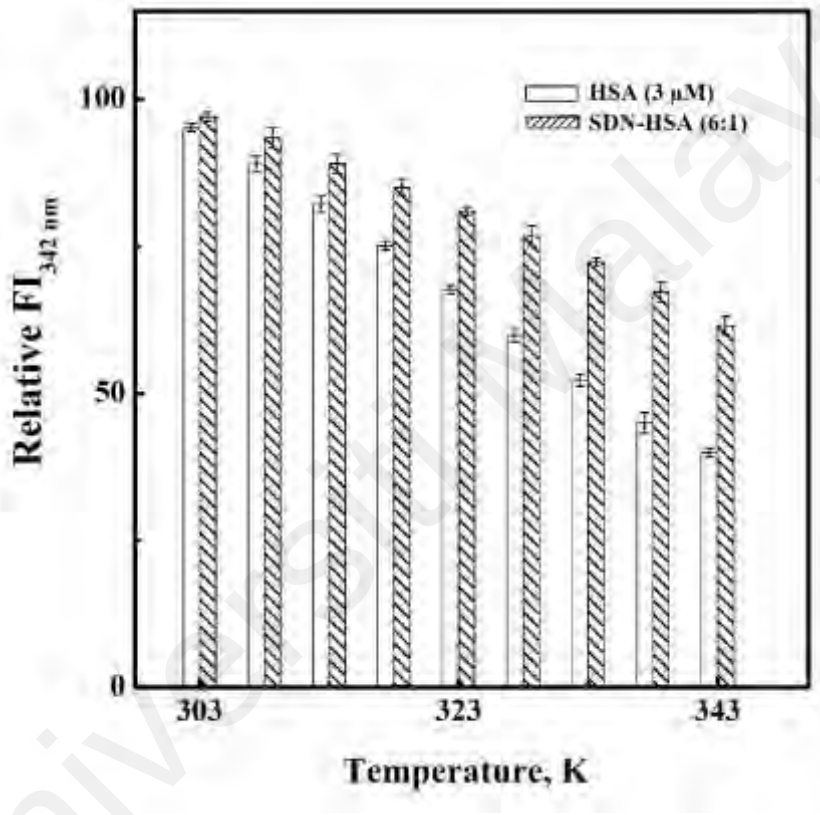

Figure 4.16: Bar diagram showing the effect of temperature on the fluorescence intensity at 342 nm ($FI_{342\ nm}$) of HSA and SDN-HSA (6:1) mixture, obtained in 60 mM sodium phosphate buffer, pH 7.4. The protein concentration was 3 μM, whereas the temperature varied in the range of 303–343 K, with 5 K intervals.

4.1.9.1 Ligand-displacement results

To locate the binding site of SDN on HSA, competitive ligand displacement experiments were conducted with the help of three different site-specific markers, *i.e.,* WFN, DZM and HMN for Sites I, II and III, respectively (Kragh-Hansen et al., 2002). Figure 4.17 depicts the fluorescence spectrum of WFN-HSA (1:1) mixture alone as well as in the presence of increasing SDN concentrations. While the fluorescence spectrum of WFN-HSA mixture was characterized by the presence of emission maxima at 383 nm (Trynda-Lemiesz, 2004), progressive reduction in the fluorescence intensity was seen with increasing SDN concentrations. The fluorescence signal of WFN-HSA complex is more specific at 383 nm and any decrease in the fluorescence intensity at 383 nm upon SDN addition was a clear indication of WFN displacement from HSA. This was a better signal than the protein fluorescence intensity at 342 nm to study WFN displacement. Figure 4.18 shows the decrease in the fluorescence intensity at 383 nm ($FI_{383\ nm}$) with increasing SDN concentrations. About 25 % reduction in the fluorescence intensity at 383 nm was noticed at 24 μM SDN concentration (Figure 4.18). Except WFN (3 μM), free SDN (24 μM), HSA (3 μM) and SDN-HSA (8:1) mixture did not produce any marked fluorescence within this range (Figure 4.17). Significant reduction in the $FI_{383\ nm}$ of WFN-HSA (1:1) mixture upon SDN addition was clear indication of the involvement of Site I for SDN binding.

The fluorescence quenching titration results of HSA alone as well as DZM-HSA (1:1) and HMN-HSA (1:1) mixtures, obtained with increasing SDN concentrations are shown in Figure 4.19 (A–C). There was significant decrease in the fluorescence intensity upon SDN addition in all cases. Although titration results were found to be qualitatively similar, quantitative differences in the magnitude of the fluorescence intensity reduction were noticed, which can be clearly seen from Figure 4.20. Therefore, the titration data were treated according to Eq. (3.6) and the resulting double logarithmic plots are shown in

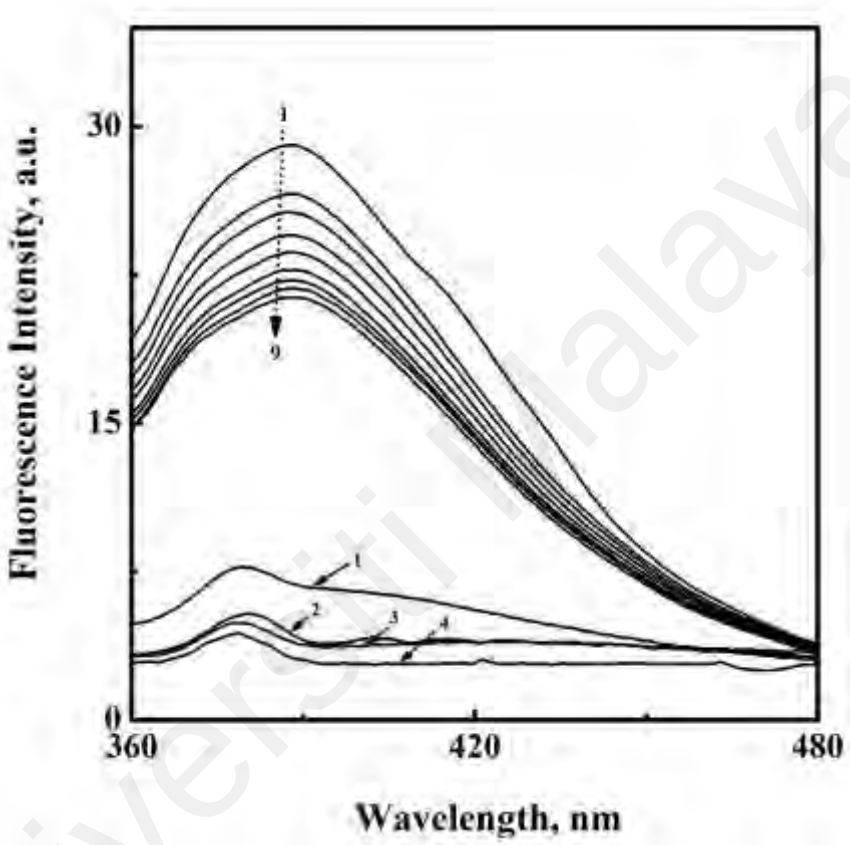

Figure 4.17: Fluorescence spectra of WFN-HSA (1:1) mixture in the absence and the presence of increasing concentrations of SDN, obtained in 60 mM sodium phosphate buffer, pH 7.4 at 298 K, upon excitation at 335 nm. The concentrations of HSA and WFN were fixed at 3 µM each while the concentration of SDN (from top to bottom, 1→9) varied as 0–24 µM with regular increments of 3 µM. Fluorescence spectra of WFN (3 µM), HSA (3 µM), SDN-HSA (8:1) mixture and SDN (24 µM) are marked as 1-4, respectively.

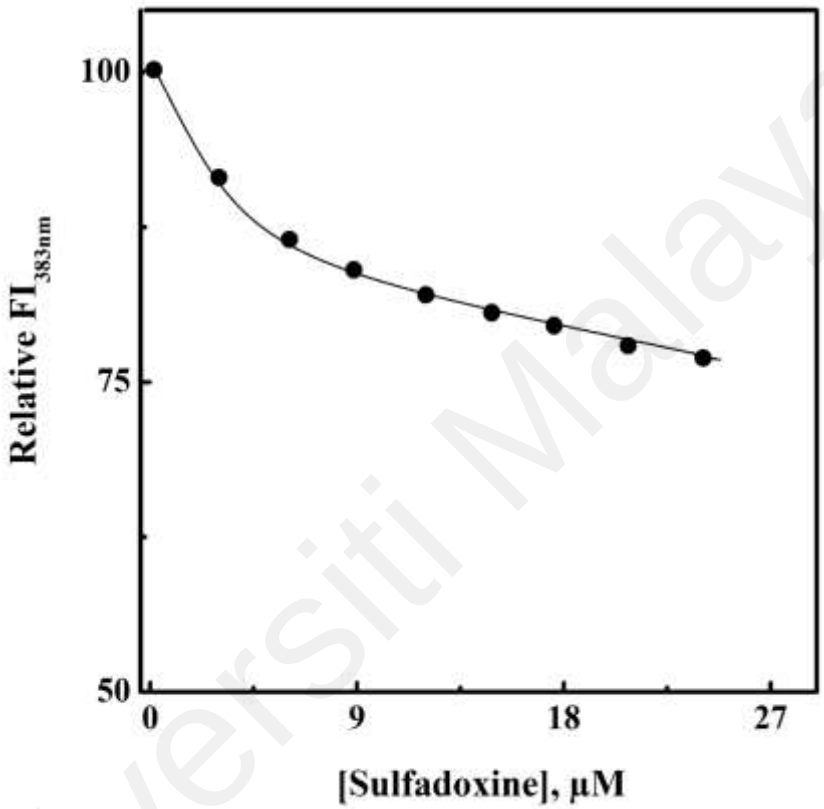

Figure 4.18: Plot showing the decrease in the relative fluorescence intensity at 383 nm (Relative $FI_{383\ nm}$) of the WFN-HSA (1:1) mixture with increasing concentrations of SDN. Values of the $FI_{383\ nm}$ at different SDN concentrations were taken from the data shown in Figure 4.17.

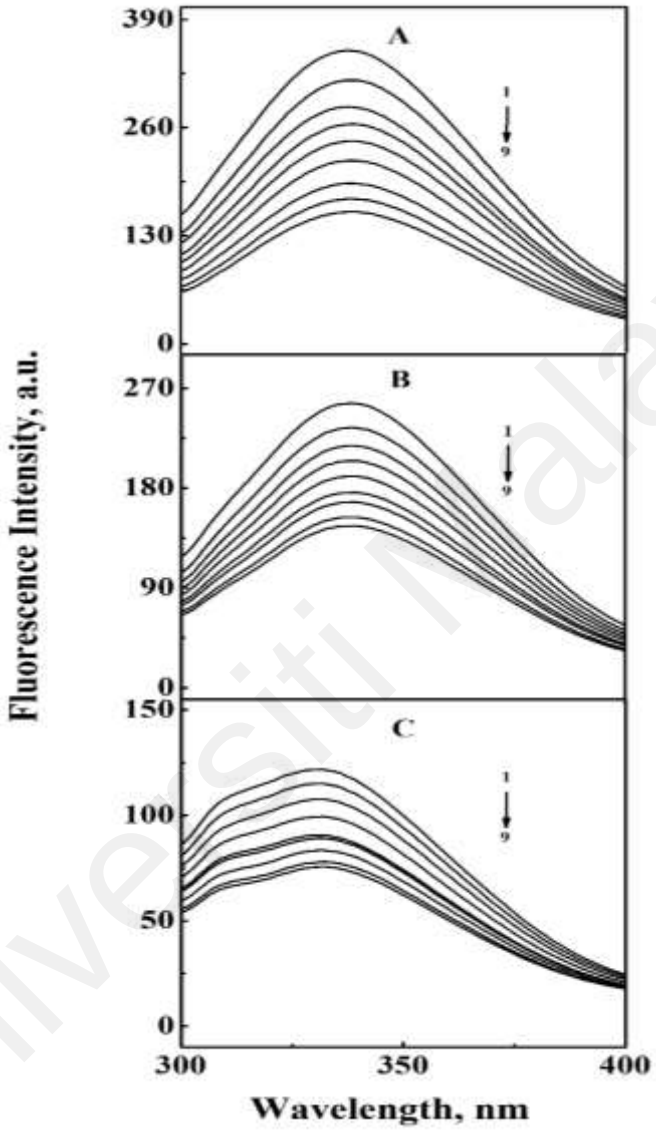

Figure 4.19: (A). Fluorescence spectra of HSA in the presence of increasing SDN concentrations. (B). Fluorescence spectra of DZM-HSA (1:1) mixture, in the presence of increasing SDN concentrations. (C). Fluorescence spectra of HMN-HSA (1:1) mixture, in the presence of increasing SDN concentrations. The protein concentration was 3 µM while the concentration of SDN (from top to bottom, 1→9) varied as 0–24 µM with regular increment of 3 µM. These spectra were obtained in 60 mM sodium phosphate buffer, pH 7.4 at 298 K, upon excitation at 280 nm.

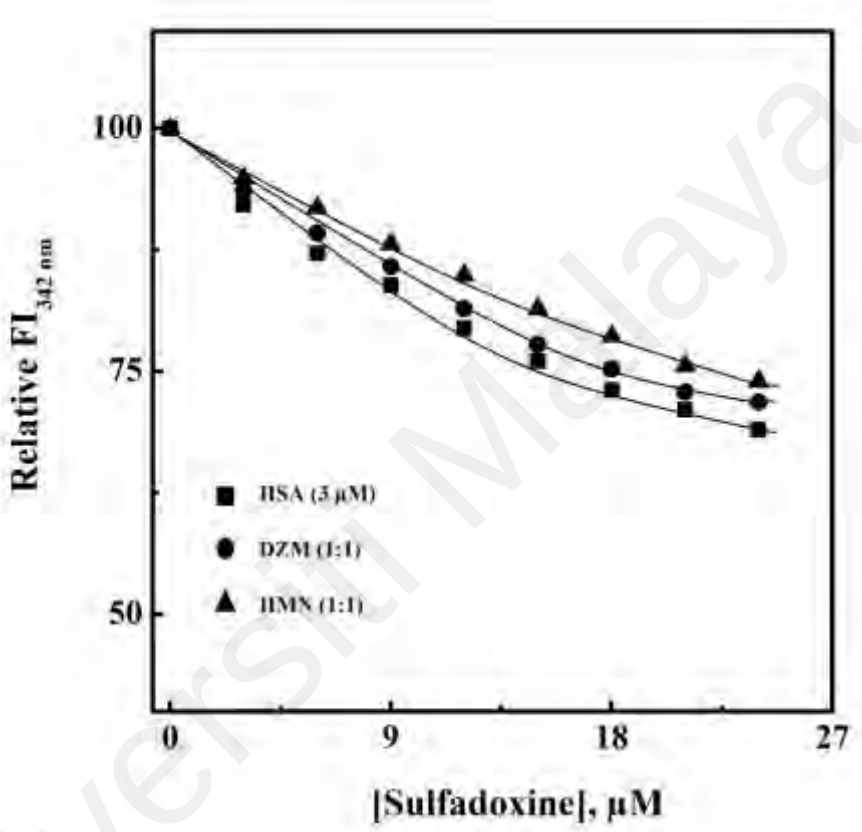

Figure 4.20: Plots showing the decrease in the relative fluorescence intensity at 342 nm (Relative $FI_{342\ nm}$) of HSA and its 1:1 mixtures with DZM and HMN upon SDN addition. The concentrations of HSA and DZM as well as HMN were fixed at 3 µM each while the SDN concentration varied in the range of 0–24 µM. Values of the $RFI_{342\ nm}$ at different SDN concentrations were taken from the data, shown in Figure 4.19.

Figure 4.21. Quantitative determination of the binding constant of SDN-HSA system in the presence of either DZM (K_a = 3.41 ± 0.05 × 10^4 M^{-1}) or HMN (K_a = 3.44± 0.07 × 10^4 M^{-1}) revealed no significant difference compared to the K_a value (3.47 ± 0.06 × 10^4 M^{-1}), obtained in their absence. These results clearly suggested non-involvement of Site II or Site III in the binding of SDN to HSA. On the other hand, Site I seemed to be the preferable binding site of SDN on HSA. This conclusion was also supported by the molecular docking results, described in the next section.

4.1.9.2 Molecular docking results

Molecular docking enabled the prediction and visualisation of generated interactions between SDN and HSA at the molecular level. The specific docking was aimed at the two well-known HSA binding sites, namely, Site I and Site II. Initial analysis showed that a total of 17 clusters were developed on Site I, while 22 clusters on Site II, based on the 100 search runs. In general, the lower number of total clusters on Site I compared to Site II indicated stricter movement of SDN on Site I than Site II. As can be visualised from Figure 4.22, the highest populated cluster on Site I consisted of 33 members with a mean binding energy of – 29.92 kJ mol^{-1}, whereas 30 members constituted the highest populated cluster at Site II with mean binding energy of –22.47 kJ mol^{-1}. Moreover, majority of the clusters generated on Site I possessed higher binding energy (more negative) than those generated on Site II of HSA. These results indicated that SDN binding affinity was leaning towards Site I of HSA. Further analysis revealed that the lowest binding energy of SDN summed on Site I was –33.26 kJ mol^{-1}, compared to –25.15 kJ mol^{-1} on Site II. These binding energy results indicated that SDN formed a more stable complex when it was bound to Site I than Site II of HSA.

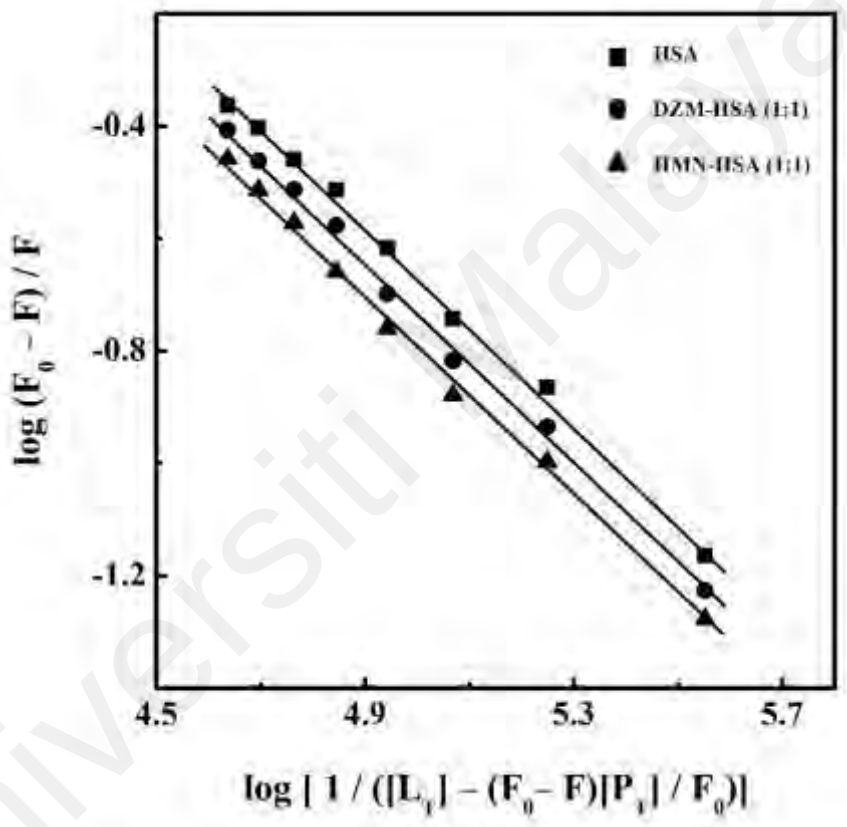

Figure 4.21: Double logarithmic plots of log ($F_0 - F$) / F against log [1 / ([L_T] − (F_0 − F) [P_T] / F_0)] of HSA and its 1:1 mixtures with DZM and HMN for the binding constant determination.

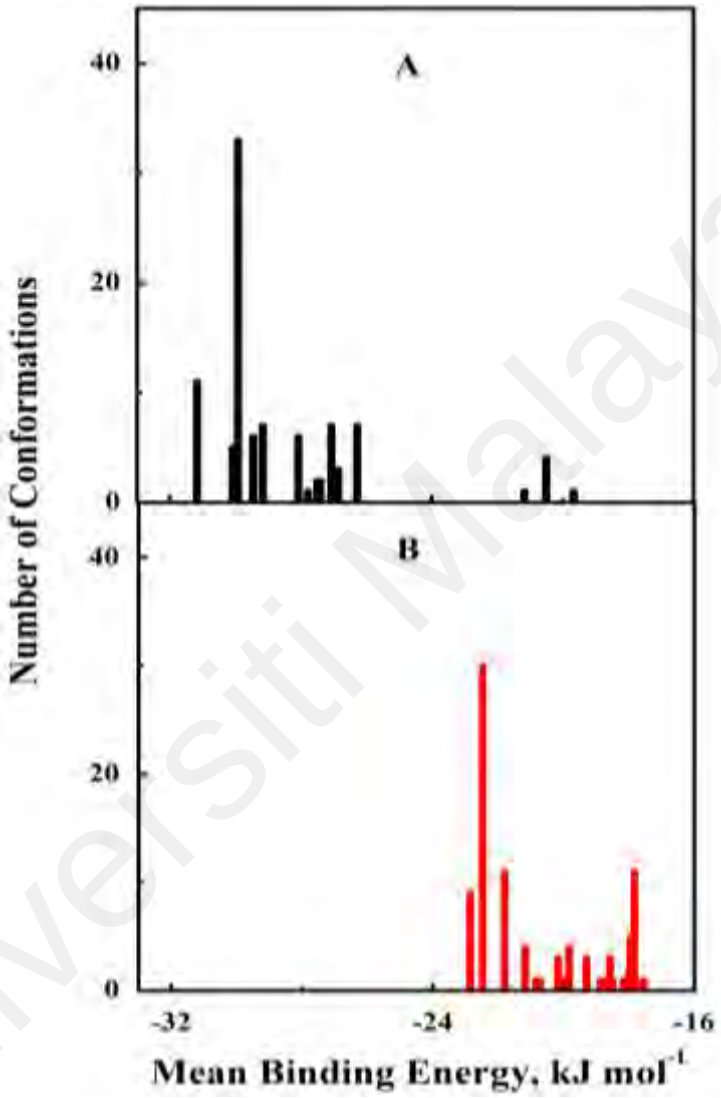

Figure 4.22: Cluster analysis showing the docking of SDN to both ligand binding sites, Site I (A) and Site II (B) of HSA. Leaning of the highest population of conformational clusters toward Site I (A) was indicative of binding preference of sulfadoxine to Sudlow's Site I of HSA compared to Site II (B).

The inspection of formed molecular interactions between HSA and SDN was done by utilizing the binding model with the lowest binding energy at Site I. As shown in Figure 4.23, SDN formed two hydrogen bonds at Site I, involving His-242 and Arg-257 residues of HSA. Furthermore, the bound SDN at Site I was surrounded by amino acid residues *Ser287, Arg222, Arg257, His242, Glu292, Lys199, Trp214, Leu238, Tyr150, Ala291* and *Leu260,* as reflected from LigPlot+ (Figure 4.24). Overall, based on the molecular docking analysis, SDN was shown to have the binding preference at Site I of HSA. These results were in line to the one obtained from ligand displacement experiments, suggesting Site I as the preferred SDN binding site.

4.1.10 Effect of metal ions on SDN-HSA system

The fluorescence quenching titration results of SDN-HSA system, obtained in presence of various metal salts were analysed and transformed into double logarithmic plots, as shown in Figure 4.25. The values of the binding constant, K_a obtained in the absence and presence of various metal salts are listed in Table 4.3. There was smaller but significant decrease in the K_a values in the presence of these metal salts, which followed the order: KCl >$MnCl_2$ / $CuCl_2$ >$BaCl_2$. On the other hand, presence of $MgCl_2$, produced a slight increase in the K_a value while no effect was seen in presence of $CaCl_2$. Such alteration in the K_a value can be ascribed either to the binding of metal ions near the SDN binding site on HSA or to SDN molecule around electronegative atoms to form a bridge between SDN and HSA. However, more experiments are needed to justify this explanation.

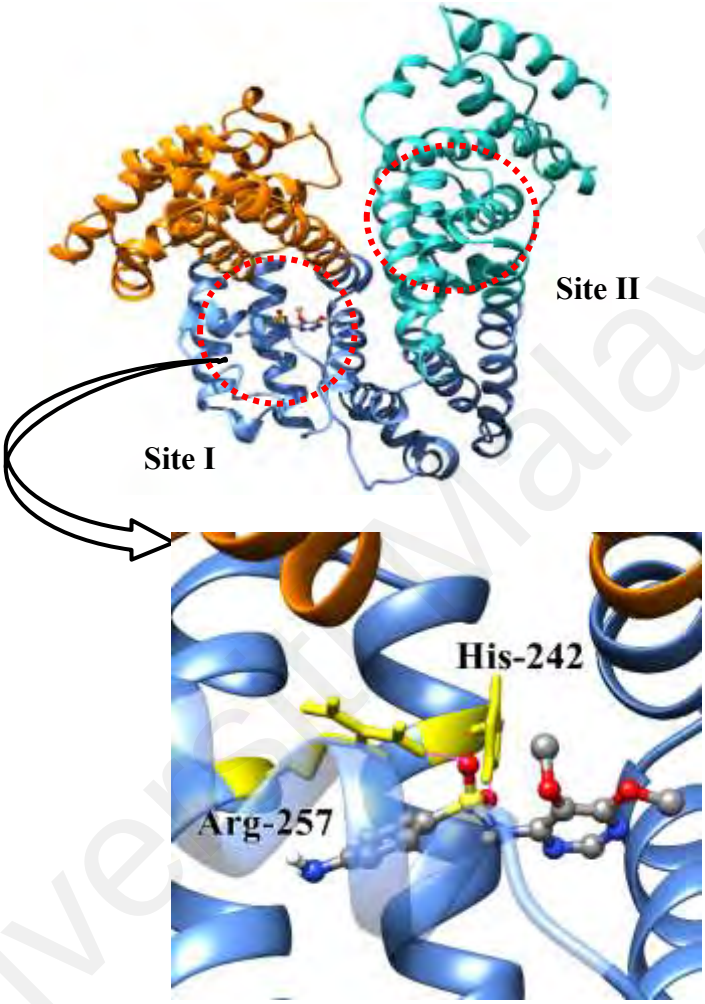

Figure 4.23: Diagram showing the predicted orientation of SDN (rendered in ball and stick) on Site I of HSA. The three domains of HSA are coloured in orange (domain I), blue (domain II), and green (domain III). The zoomed-in image shows the formed hydrogen bonds (pink lines) between the amino acid residues of HSA (rendered in yellow stick) and SDN at Site I.

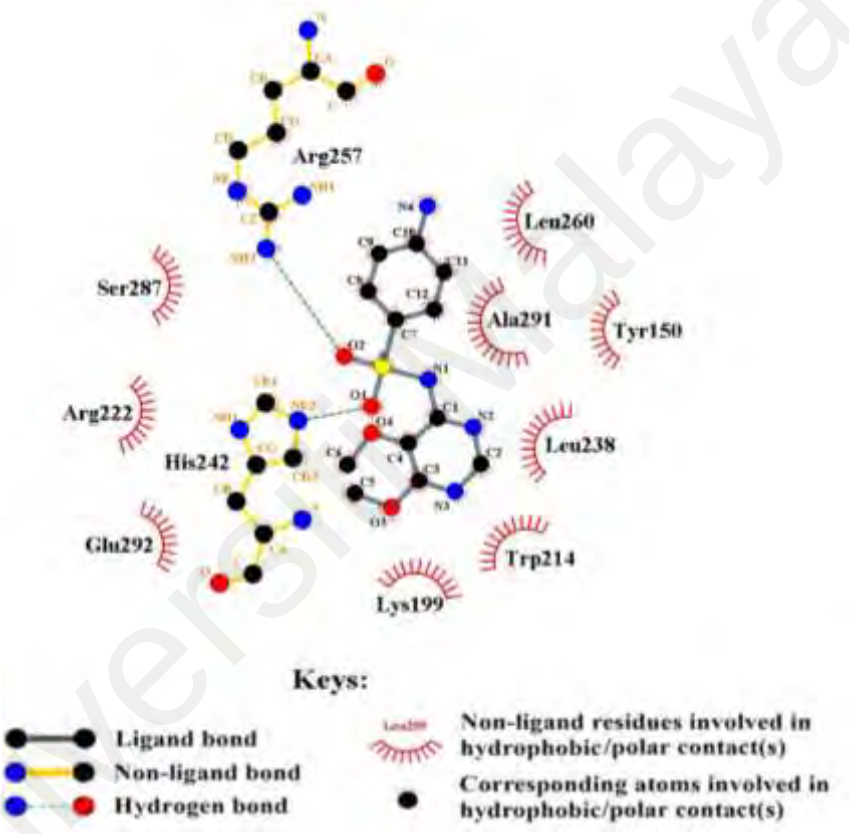

Figure 4.24: LigPlot+ diagram showing hydrophobic interactions between SDN (grey) atoms and the amino acid residues of HSA at Site I.

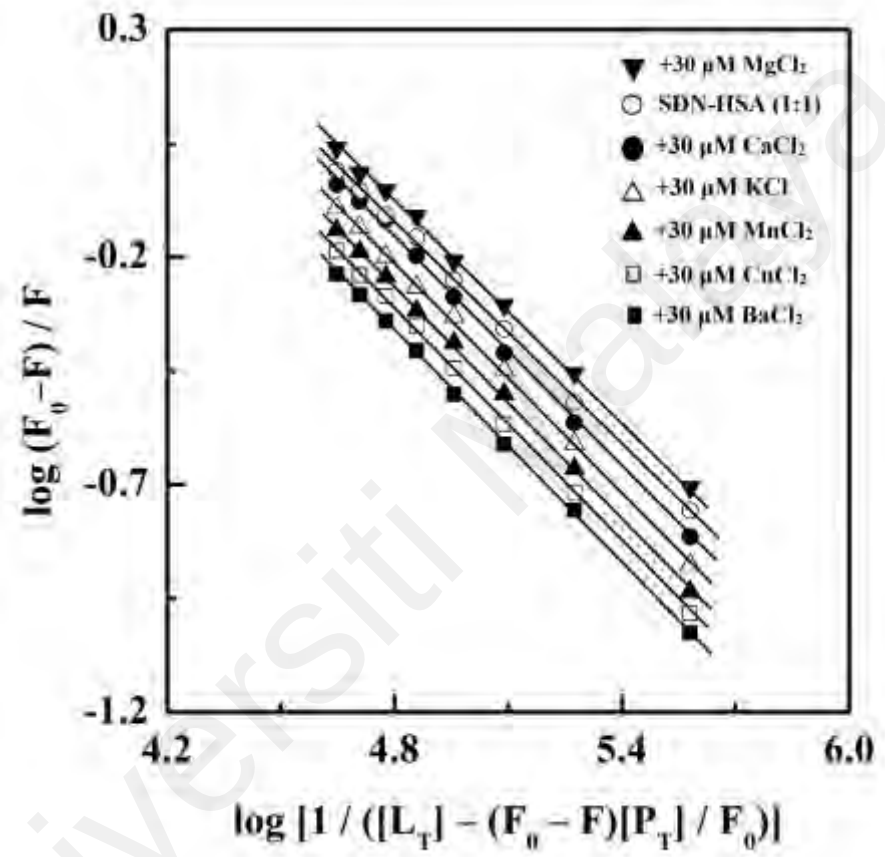

Figure 4.25: Double logarithmic plots of log ($F_0 - F$) / F against log [1 / ([L_T] – (F_0 – F) [P_T] / F_0)] for SDN–HSA system in the presence of different metal salts, obtained in 60 mM sodium phosphate buffer, pH 7.4. The concentrations of the protein and the metal salts ($MgCl_2$, KCl, $CaCl_2$, $MnCl_2$, $CuCl_2$ and $BaCl_2$) were fixed as 3 µM and 30 µM, respectively, while concentrations of SDN varied as 3− 24 µM with regular increments of 3 µM.

Table 4.3: Values of the binding constant, K_a for SDN-HSA binding reaction in the absence and the presence of different metal salts.

Metal salts	$K_a \times 10^4$ (M^{-1})
-	3.49 ± 0.02
$MgCl_2$	4.07 ± 0.19
KCl	3.29 ± 0.01
$CaCl_2$	3.41 ± 0.11
$MnCl_2$	3.17 ± 0.09
$CuCl_2$	3.09 ± 0.06
$BaCl_2$	2.53 ± 0.13

CHAPTER 5: CONCLUSION

From these findings, the complex formation between SDN and HSA was affirmed based on the spectroscopic and voltammetric techniques and was well supported by the molecular docking results. A moderate binding affinity (3.49×10^4 M^{-1}) between SDN and HSA involving hydrophobic interactions, as predicted from the thermodynamic data (ΔS = +104.42 J mol^{-1} K^{-1}, ΔH = +5.25 kJ mol^{-1}) stabilized the SDN-HSA complex. This binding produced slight alteration in the microenvironment around protein fluorophores but increased protein's thermal stability. SDN preferred to occupy Site I, located in subdomain IIA of HSA. Small alteration in the K_a value, reflecting smaller change in the binding affinity was also noticed in the presence of a few metal ions. These results will aid in the understanding of the pharmacokinetics and further development of the drug.

REFERENCES

Abou-Zied, O. K., & Al-Shihi, O. I. (2008). Characterization of subdomain IIA bi site of human serum albumin in its native, unfolded, and refolded states small molecular probes. *Journal of American Chemical Society*, *130*, 10793–10801.

Aronson, J. K. (2003). *Side effects of drugs annual* (1st ed.). London, United Kingdom: Elsevier.

Aucamp, M., Milne, M., & Liebenberg, W. (2016). Amorphous sulfadoxine: A physical stability and crystallization kinetics study. *American Association of Pharmaceutical Scientists, 17*(5), 1100–1109.

Ayranci, E., & Duman, O. (2004). Binding of fluoride, bromide and iodide to bovine serum albumin, studied with ion-selective electrodes. *Food Chemistry*, *84*, 539–543.

Baig, M. H., Rahman, S., Rabbani, G., Imran, M., Ahmad, K., & Choi, I. (2019). Multi-spectroscopic characterization of human serum albumin binding with cyclobenzaprine hydrochloride: Insights from biophysical and *in silico* approaches. *International Journal of Molecular Sciences*, *20*(3), Article #662.

Bertucci, C., & Domenici, E. (2002). Reversible and covalent binding of drugs to human serum albumin: Methodological approaches and physiological relevance. *Current Medicinal Chemistry*, *9*(15), 1463–1481.

Bloland, P. B. (2003). A contrarian view of malaria therapy policy in Africa. *The American Journal of Tropical Medicine and Hygiene*, *68*(2), 125–126.

Bos, O. J., Remijn, J. P., Fischer, M. J., Wilting, J., & Janssen, L. H. (1988). Location and characterization of the warfarin binding site of human serum albumin: A comparative study of two large fragments. *Biochemical Pharmacology*, *37*(20), 3905–3909.

Brand. L., & Johnson, M. L. (2008). Fluorescence Spectroscopy. *Methods in Enzymology*. (1st ed.). Maryland, USA: Elsevier.

Brodersen, R., Sjödin, T., & Sjöholm, I. (1977). Independent binding of ligands to human serum albumin. *Journal of Biology Chemistry*, *252*, 5067–5072.

Bi, S.Y., Ding, L., Tian, Y., Song, D. Q., Zhou, X., Liu, X., & Zhang, H. Q. (2004). Investigation of the interaction between flavonoids and human serum albumin. *Journal of Molecular Structure*, *703*, 37–45.

Bijari, N., Shokoohinia, Y., Ashrafi-Kooshk, M. R., Ranjbar, S., Parvaneh, S., Moieni-Arya, M., & Khodarahmi, R. (2013). Spectroscopic study of interaction between osthole and human serum albumin: Identification of possible binding site of the compound. *Journal of Luminescence*, *143*, 328–336.

Bunnag, D., Karbwang, J., Na-Bangchang, K., Thanavibul, A., Chittamas, S., & Harinasuta, T. (1996). Quinine-tetracycline for multidrug resistant falciparum

malaria. *The Southeast Asian Journal of Tropical Medicine and Public Health*, *27*(1), 15–18.

Carter, D. C., He, X. M., Munson, S. H., Twigg, P. D., Gernert, K. M., Broom, M. B., & Miller, T. Y. (1989). Three-dimensional structure of human serum albumin. *Science*, *244*(4909), 1195–1198.

Carter, D. C., & Ho, J. X. (1994). Structure of serum albumin. *Advances in Protein Chemistry, 45,* 153–203.

Carter, D. C., Ho, J., & Wang, Z. (2007). *U.S. Patent Application No. 10/577,943*.

Carter, R., & Mendis, K. N. (2003). Evolutionary and historical aspects of the burden of Malaria. *Clinical Microbiology Reviews*, *16*(1), Article #173.

Carter, D. C. (2010). Crystallographic survey of albumin drug interaction and preliminary applications in cancer chemotherapy. In D. J. Abraham & D. P Rotella (Eds.), Burger's medicinal chemistry and drug discovery (pp. 437–467). New York, NY; John Wiley & Sons, Inc.

Celej, M. S., Montich, G. G., & Fidelio, G. D. (2003). Protein stability induced by ligand binding correlates with changes in protein flexibility. *Protein Science*, *12*, 1496–1506.

Chadha, N., Singh, D., Milton, M. D., Mishra, G., Daniel, J., Mishra, A. K., & Tiwari, A. K. (2020). Computational prediction of interaction and pharmacokinetics profile study for polyamino-polycarboxylic ligands on binding with human serum albumin. *New Journal of Chemistry*, *44*(7), 2907–2918.

Chaves, O. A., Amorim, A. P. D. O., Castro, L. H., Sant'Anna, C. M. R., De Oliveira, M. C., Cesarin-Sobrinho, D., ... Ferreira, A. B. (2015). Fluorescence and docking studies of the interaction between human serum albumin and pheophytin. *Molecules*, *20*(10), 19526–19539.

Chaves, O. A., Tavares, M. T., Cunha, M. R., Parise-Filho, R., Sant'Anna, C. M. R., & Netto-Ferreira, J. C. (2018). Multi-Spectroscopic and theoretical analysis on the interaction between human serum albumin and a capsaicin derivative-RPF101. *Biomolecules*, *8*(3), Article #78.

Chen, Y. H., Yang, J. T., & Martinez, H. M. (1972). Determination of the secondary structures of proteins by circular dichroism and optical rotatory dispersion. *Biochemistry*, *11*, 4120–4131.

Chen, Y., & Barkley, M. D. (1998). Toward understanding tryptophan fluorescence in proteins. *Biochemistry*, *37*, 9976–9982.

Chi, Z., Liu, R., Teng, Y., Fang, X., & Gao, C. (2010). Binding of oxytetracycline to bovine serum albumin: Spectroscopic and molecular modelling investigations. *Journal of Agricultural and Food Chemistry*, *58*(18), 10262–10269.

Choemang, A., & Na-Bangchang, K. (2019). An alternative HPLC with ultraviolet detection for determination of piperaquine in plasma. *Journal of Chromatographic Science*, *57*(1), 27–32.

Chuang, V. T. G., & Otagiri, M. (2001). Flunitrazepam, a 7-nitro-1, 4-benzodiazepine that is unable to bind to the indole-benzodiazepine site of human serum albumin. *Biochimica et Biophysica Acta - Protein Structure and Molecular Enzymology*, *1546*(2), 337–345.

Chulay, J. D., Watkins, W. M., & Sixsmith, D. G. (1984). Synergistic antimalarial activity of pyrimethamine and sulfadoxine against *Plasmodium falciparum in vitro*. *The American Journal of Tropical Medicine and Hygiene*, *33*(3), 325–330.

Coombs, G. H., Goldberg, D. E., Klemba, M., Berry, C., Kay, J., & Mottram, J. C. (2001). Aspartic proteases of *Plasmodium falciparum* and other parasitic protozoa as drug targets. *Trends in Parasitology*, *17*(11), 532–537.

Cosgriff, T. M., Boudreau, E. F., Pamplin, C. L., Doberstyn, E. B., Desjardins, R. E., & Canfield, C. J. (1982). Evaluation of the antimalarial activity of the phenanthrenemethanol halofantrine. *The American Journal of Tropical Medicine and Hygiene*, *31*(6), 1075–1079.

Cox-Singh, J., & Singh, B. (2008). *Knowlesi* malaria: Newly emergent and of public health importance. *Trends in Parasitology*, *24*(9), 406–410.

Curry, S. (2009). Lessons from the crystallographic analysis of small molecules binding to human serum albumin. *Drug Metabolism and Pharmacokinetics, 24,* 342–357.

Della Porta, V., Bramanti, E., Campanella, B., Tiné, M. R., & Duce, C. (2016). Conformational analysis of bovine serum albumin adsorbed on halloysite nanotubes and kaolinite: A Fourier transform infrared spectroscopy study. *RSC Advances*, *6*(76), 72386–72398.

De Kock, M., Tarning, J., Workman, L., Nyunt, M. M., Adam, I., Barnes, K. I., & Denti, P. (2017). Pharmacokinetics of sulfadoxine and pyrimethamine for intermittent preventive treatment of malaria during pregnancy and after delivery. *Pharmacometrics and Systems Pharmacology*, *6*(7), 430–438.

Deloron, P., Bertin, G., Briand, V., Massougbodji, A., & Cot, M. (2010). Sulfadoxine/pyrimethamine intermittent preventive treatment for malaria during pregnancy. *Emerging Infectious Diseases*, *16*(11), Article #1666.

Dockal, M., Carter, D. C., & Rüker, F. (1999). The three recombinant domains of human serum albumin structural characterization and ligand binding properties. *Journal of Biological Chemistry*, *274*(41), 29303–29310.

Dugaiczyk, A., Law, S. W., & Dennison, O. E. (1982). Nucleotide sequence and the encoded amino acids of human serum albumin mRNA. *Proceedings of the National Academy of Sciences, USA, 79*, 71–75.

Eastman, R. T., & Fidock, D. A. (2009). Artemisinin-based combination therapies: A vital tool in efforts to eliminate malaria. *Nature Reviews Microbiology*, *7*(12), 864–874.

Edozien, J. C., Gilles, H. M., & Udeozo, I. O. K. (1962). Adult and cord-blood gamma-globulin and immunity to malaria in Nigerians. *Lancet*, *95*, 1–5.

Elgawish, M. S., Soltan, M. K., & Sebaiy, M. M. (2019). Molecular modeling, spectrofluorimetric, and tandem mass spectrometric analysis reveal a competitive binding of amlodipine and rosuvastatin to plasma albumin: Insight into drug-drug interaction. *Microchemical Journal*, *149,* Article #104014.

Erhirhie, E. A. (2006). Antimalarial therapies and infertility: A comprehensive review. *Toxicology International, 23*(2), 107–111.

Eyasu, M. (2015). Antimalarial drug resistance: In the past, current status and future perspectives. *British Journal of Pharmacology and Toxicology*, *6*(1), 1–15.

Farrar, J., Hotez, P. J., Junghanss, T., Kang, G., Lalloo, D., & White, N. J. (2013). *Manson's Tropical Diseases* (23rd ed.). Oxford, United Kingdom: Elsevier Health Sciences.

Fasano, M., Fanali, G., Leboffe, L., & Ascenzi, P. (2007). Heme binding to albuminoid proteins is the result of recent evolution. *IUBMB Life, 59*, 436–440.

Fehske, K. J., Schläfer, U., Wollert, U., & Müller, W. E. (1982). Characterization of an important drug binding area on human serum albumin including the high-affinity binding sites of warfarin and azapropazone. *Molecular Pharmacology*, *21*(2), 387–393.

Feroz, S. R., Malek, S. N. A., & Tayyab, S. (2016). Characteristics and thermodynamics of the interaction of 6-shogaol with human serum albumin as studied by isothermal titration calorimetry. *Brazilian Journal of Pharmaceutical Sciences*, *52*, 443–446.

Figge, J., Rossing, T., & Fencl, V. (1991). The role of serum proteins in acid-base equilibria. *The Journal of Laboratory and Clinical Medicine, 117*(6), 453–467.

Foley, M., & Tilley, L. (1997). Quinoline antimalarials: Mechanisms of action and resistance. *International Journal for Parasitology*, *27*(2), 231–240.

Gatton, M. L., Martin, L. B., & Cheng, Q. (2004). Evolution of resistance to sulfadoxine-pyrimethamine in *Plasmodium falciparum*. *Antimicrobial Agents and Chemotherapy*, *48*(6), 2116–2123.

Gelband, H., Panosian, C. B., & Arrow, K. J. (2004). Saving lives, buying time: Economics of malaria drugs in an age of resistance. Washington, DC: National Academies Press.

Ghuman, J., Zunszain, P. A., Petitpas, I., Bhattacharya, A. A., Otagiri, M., & Curry, S. (2005). Structural basis of the drug-binding specificity of human serum albumin. *Journal of Molecular Biology*, *353*(1), 38–52.

Goncharov, N. V., Belinskaia, D. A., Shmurak, V. I., Terpilowski, M. A., Jenkins, R. O., & Avdonin, P. V. (2017). Serum albumin binding and esterase activity: Mechanistic interactions with organophosphates. *Molecules, 22*(7), Article #1201.

Greenfield, N. J. (2006). Using circular dichroism spectra to estimate protein secondary structure. *Nature Protocols*, *1*, 2876–2890.

Greenwood, B., & Mutabingwa, T. (2002). Malaria in 2002. *Nature*, *415*, 670–672.

Gregson, A., & Plowe, C. V. (2005). Mechanisms of resistance of malaria parasites to antifolates. *Pharmacological Reviews*, *57*(1), 117–145.

Halgren, T. A. (1996). Merck molecular force field. I. Basis, form, scope, parameterization, and performance of MMFF94. *Journal of Computational Chemistry, 17*, 490–519.

Hanwell, M. D., Curtis, D. E., Lonie, D. C., Vandermeersch, T., Zurek, E., & Hutchison, G. R. (2012). Avogadro: An advanced semantic chemical editor, visualization, and analysis platform. *Journal of Cheminformatics*, *4*, Article #17.

He, X. M., & Carter, D. C. (1992). Atomic structure and chemistry of human serum albumin. *Nature*, *358*(6383), 209–215.

Hosseinzadeh, R., & Khorsandi, K. (2016). Interaction of vitamin B1 with bovine serum albumin investigation using vitamin B1-selective electrode: Potentiometric and molecular modeling study. *Journal of Biomolecular Structure and Dynamics*, *34*(9), 1903–1910.

Hu, W., Luo, Q., Wu., K., Li, X., Wang, F., Chen, Y., … Sadler, P. J. (2011). The anticancer drug cisplatin can cross-link the interdomain zinc site on human albumin. *Chemical Communications*, *47*(21), 6006–6008.

Hunter, M. J. (1966). A method for the determination of protein partial specific volumes. *The Journal of Physical Chemistry, 70*(10), 3285–3292.

Hyde, J. E. (2005). Exploring the folate pathway in *Plasmodium falciparum*. *Acta Tropica*, *94*(3), 191–206.

Jamei, M., Dickinson, G. L., & Rostami-Hodjegan, A. (2009). A framework for assessing inter-individual variability in pharmacokinetics using virtual human populations and integrating general knowledge of physical chemistry, biology, anatomy, physiology and genetics: A tale of 'bottom-up' Vs 'top-down' recognition of covariates. *Drug Metabolism and Pharmacokinetics, 24*(1), 53–75.

Jarcho, S. (1984). Laveran's discovery in the retrospect of a century. *Bulletin of the History of Medicine*, *58*(2), 215–224.

Jirgensons, B. (1955). The intrinsic viscosity of serum albumin. *Macromolecular Chemistry and Physics*, *16*(1), 192–197.

Kabir, M. Z., Tee, W. V., Mohamad, S. B., Alias, Z., & Tayyab, S. (2016). Interaction of an anticancer drug, gefitinib with human serum albumin: Insights from fluorescence spectroscopy and computational modeling analysis. *RSC Advances*, *6*(94), 91756–91767.

Kabir, M. Z., Tee, W. V., Mohamad, S. B., Alias, Z., & Tayyab, S. (2017). Comprehensive insight into the binding of sunitinib, a multitargeted anticancer drug, to human serum albumin. *Spectrochimica Acta Part A: Molecular and Biomolecular Spectroscopy*, *181*, 254–263.

Kapoor, V. K. (1988). Sulfadoxine. *Analytical Profiles of Drug Substances*, *17*, 571–605.

Kayentao, K., Garner, P., van Eijk, A. M., Naidoo, I., Roper, C., Mulokozi, A., ... TerKuile, F. O. (2013). Intermittent preventive therapy for malaria during pregnancy using 2 Vs 3 or more doses of sulfadoxine-pyrimethamine and risk of low birth weight in Africa: Systematic review and meta-analysis. *Journal of the American Medical Association*, *309*(6), 594–604.

Keen, P. (1971). Effect of binding to plasma proteins on the distribution, activity and elimination of drugs. *In Concepts in Biochemical Pharmacology* (Vol. 28. pp. 213–233). Berlin, Heidelberg: Springer.

Kelly, S. M., & Price, N. C. (1997). The application of circular dichroism to studies of protein folding and unfolding. *Biochimica et Biophysica Acta*, *1338*, 161–185.

Kelly, S. M., Jess, T. J., & Price, N. C. (2005). How to study proteins by circular dichroism. *Biochimica et Biophysica Acta*, *1751*, 119–139.

Klayman, D. L., Lin, A. J., Acton, N., Scovill, J. P., Hoch, J. M., Milhous, W. K., ... Dobek, A. S. (1984). Isolation of artemisinin (qinghaosu) from *Artemisia annua* growing in the United States. *Journal of Natural Products*, *47*(4), 715–717.

Kragh-Hansen, U. (1985). Relations between high-affinity binding sites of markers for binding regions on human serum albumin. *Biochemical Journal, 225*, 629–638.

Kragh-Hansen, U. (1988). Evidence for a large and flexible region on human serum albumin possessing high affinity binding sites for salicylate, warfarin and other ligands. *Molecular Pharmacology, 34*, 160–171.

Kragh-Hansen, U., Chuang, V. T. G., & Otagiri, M. (2002). Practical aspects of the ligand-binding and enzymatic properties of human serum albumin. *Biological and Pharmaceutical Bulletin*, *25*(6), 695–704.

Lakowicz, J.R. (2006). *Principles of fluorescence spectroscopy* (3rd ed.). New York**:** Springer.

Larsen, M. T., Kuhlmann, M., Hvam, M. L., & Howard, K. A. (2016). Albumin-based drug delivery: Harnessing nature to cure disease. *Molecular and Cellular Therapies*, *4*(1), 1–12.

Laveran, C. L. A., Kean, B. H., Mott, K. E., & Russell, A. J. (1982). A newly discovered parasite in the blood of patients suffering from malaria. Parasitic etiology of attacks of malaria. *Reviews of Infectious Diseases*,*4*(4), 908–911.

Le Bras, J., & Durand, R. (2003). The mechanisms of resistance to antimalarial drugs in *Plasmodium falciparum*. *Fundamental & Clinical pharmacology*, *17*(2), 147–153.

Lindup, W. E., & Orme, M. C. (1981). Clinical pharmacology: Plasma protein binding of drugs. *British Medical Journal, 282*(6259), Article #212.

Liu, C., Liu, Z., & Wang, J. (2017). Uncovering the molecular and physiological processes of anticancer leads binding human serum albumin: A physical insight into drug efficacy. *PloS ONE*, *12*(4), Article #0176208.

Loeb, F., Clark, W. M., Coatney, G. R., Coggeshall, L. T., Dieuaide, F. R., Dochez, A. R., ... Sapero, J. J. (1946). Activity of a new antimalarial agent, chloroquine (SN 7618): Statement approved by the Board for coordination of malarial studies. *Journal of the American Medical Association*, *130*(16), 1069–1070.

Lu, Z. X., Cui, T., & Shi, Q. L. (1987). *Applications of circular dichroism and optical rotatory dispersion in molecular biology* (1st ed.). China**:** Science Press.

Ma, R., Guo, D. X., Li, H. F., Liu, H. X., Zhang, Y. R., Ji, J. B., … Wang, S. Q. (2019). Spectroscopic methodologies and molecular docking studies on the interaction of antimalarial drug piperaquine and its metabolites with human serum albumin. *Spectrochimica Acta Part A: Molecular and Biomolecular Spectroscopy*, *222*, Article #117158.

Maddison, J. E., Watson, A. D., & Elliott, J. (2008). Antibacterial drugs. In J. E. Maddison, S. W. Page & D. B. Church (Eds.), Small animal clinical pharmacology (pp. 148–185). Hertfordshire, United Kingdom: Elsevier.

Magdum, P. A., Gokavi, N. M., & Nandibewoor, S. T. (2017). Study on the interaction between anti-tuberculosis drug ethambutol and bovine serum albumin: Multispectroscopic and cyclic voltammetric approaches. *Luminescence*, *32*, 206–216.

Makarska-Bialokoz, M., & Lipke, A. (2019). Study of the binding interactions between uric acid and bovine serum albumin using multiple spectroscopic techniques. *Journal of Molecular Liquids*, *276*, 595-604.

Marsh, K. (1992). Malaria-a neglected disease?. *Parasitology*, *104*(S1), 53–69.

Massele, A. Y., Sayi, J., Nsimba, S. E., Ofori-Adjei, D., & Laing, R. O. (1993). Knowledge and management of malaria in Dar es Salaam, Tanzania. *East African Medical Journal*, *70*(10), 639–642.

Maurya, N., Maurya, J. K., Singh, U. K., Dohare, R., Zafaryab, M., Alam, M., M., ... Patel, R. (2019). *In vitro* cytotoxicity and interaction of noscapine with human serum albumin: Effect on structure and esterase activity of HSA. *Molecular Pharmaceutics*, *16*(3), 952–966.

McGregor, I. A. (1974). Mechanisms of acquired immunity and epidemiological patterns of antibody responses in malaria in man. *Bulletin of the World Health Organization*, *50*(3–4), Article #259.

Mendis, K., Rietveld, A., Warsame, M., Bosman, A., Greenwood, B., & Wernsdorfer, W. H. (2009). From malaria control to eradication: The WHO perspective. *Tropical Medicine & International Health*, *14*(7), 802–809.

Mikomangwa, W. P., Minzi, O., Mutagonda, R., Baraka, V., Mlugu, E. M., Aklillu, E., & Kamuhabwa, A. A. (2020). Effect of sulfadoxine-pyrimethamine doses for

prevention of malaria during pregnancy in hypoendemic area in Tanzania. *Malaria Journal*, *19*, 1–11.

Minghetti, P. P., Ruffner, D. E., Kuang, W. J., Dennison, O. E., Hawkins, J. W., Beattie, W. G., & Dugaiczyk, A. (1986). Molecular structure of the human albumin gene is revealed by nucleotide sequence within q11-22 of chromosome 4. *Journal of Biological Chemistry*, *261*(15), 6747–6757.

Mlugu, E. M., Minzi, O., Asghar, M., Färnert, A., Kamuhabwa, A. A., & Aklillu, E. (2020). Effectiveness of sulfadoxine-pyrimethamine for intermittent preventive treatment of malaria and adverse birth outcomes in pregnant women. *Pathogens*, *9*(3), Article #207.

Mocz, G., & Ross, J. A. (2013). Fluorescence techniques in analysis of protein-ligand interactions. *Methods in Molecular Biology*, *1008*, 169–210.

Mohan, K., & Stevenson, M. M. (1998). Acquired immunity to asexual blood stages. In I. W. Shermen (Ed.), Malaria: Parasite biology, pathogenesis, and protection. (pp. 467–493). Washington, DC: American Society for Microbiology.

Möller, M., & Denicola, A. (2002). Protein tryptophan accessibility studied by fluorescence quenching. *Biochemistry and Molecular Biology Education*, *30*, 175–178.

Moore, D. V., & Lanier, J. E. (1961). Observations on two *Plasmodium falciparum* infections with an abnormal response to chloroquine. *The American Journal of Tropical Medicine and Hygiene*, *10*(1), 5–9.

Morris, G. M., Huey, R., Lindstrom, W., Sanner, M. F., Belew, R. K., Goodsell, D. S., & Olson, A. J. (2009). Autodock4 and AutoDockTools4: Automated docking with selective receptor flexibility. *Journal of Computational Chemistry*, *30*, 2785–2791.

Mousavi, S. F., & Fatemi, M. H. (2019). Probing the binding mechanism of capecitabine to human serum albumin using spectrometric methods, molecular modeling, and chemometrics approach. *Bioorganic Chemistry*, *90*, Article #103037.

Musa, K. A., Ridzwan, N. F. W., Mohamad, S. B., & Tayyab, S. (2020). Exploring the combination characteristics of lumefantrine, an antimalarial drug and human serum albumin through spectroscopic and molecular docking studies. *Journal of Biomolecular Structure and Dynamics*. Retrieved on 28 July 2020 from https://doi.org/10.1080/07391102.2020.1713215.

Mutabingwa, T. K., Anthony, D., Heller, A., Hallett, R., Ahmed, J., Drakeley, C., … Whitty, C. J. (2005). Amodiaquine alone, amodiaquine+sulfadoxine-pyrimethamine, amodiaquine+artesunate, and artemether-lumefantrine for outpatient treatment of malaria in Tanzanian children: A four-arm randomised effectiveness trial. *The Lancet*, *365*(9469), 1474–1480.

Nevídalová, H., Michalcová, L., & Glatz, Z. (2018). In-depth insight into the methods of plasma protein-drug interaction studies: Comparison of capillary electrophoresis-

frontal analysis, isothermal titration calorimetry, circular dichroism and equilibrium dialysis. *Electrophoresis*, *39*(4), 581–589.

Newman, R. D., Hailemariam, A., Jimma, D., Degifie, A., Kebede, D., Rietveld, A. E., ... Parise, M. E. (2003). Burden of malaria during pregnancy in areas of stable and unstable transmission in Ethiopia during a nonepidemic year. *The Journal of Infectious Diseases*, *187*(11), 1765–1772.

Nzila, A., Ward, S. A., Marsh, K., Sims, P. F., & Hyde, J. E. (2005). Comparative folate metabolism in humans and malaria parasites (part I): Pointers for malaria treatment from cancer chemotherapy. *Trends in Parasitology*, *21*, 292–298.

Ojingwa, J. C., Spahn-Langguth, H., & Benet, L. Z. (1994). Reversible binding of tolmetin, zomepirac, and their glucuronide conjugates to human serum albumin and plasma. *Journal of Pharmacokinetics and Biopharmaceutics*, *22*(1), 19–40.

Okell, L. C., Drakeley, C. J., Ghani, A. C., Bousema, T., & Sutherland, C. J. (2008). Reduction of transmission from malaria patients by artemisinin combination therapies: A pooled analysis of six randomized trials. *Malaria Journal*, *7*(1), Article #125.

Olson, R. E., & Christ, D. D. (1996). Plasma protein binding of drugs. *Annual Reports in Medicinal Chemistry*, *31*, 327–336.

Oncley, J. L., Scatchard, G., & Brown, A. (1947). Physical-chemical characteristics of certain of the proteins of normal human plasma. *The Journal of Physical Chemistry*, *51*(1), 184–198.

Oravcova, J., Bo, B., & Lindner, W. (1996). Drug-protein binding studies new trends in analytical and experimental methodology. *Journal of Chromatography B: Biomedical Sciences and Applicatios*, *677*, 1–28.

Otagiri, M. (2005). A molecular functional study on the interactions of drugs with plasma proteins. *Drug Metabolism and Pharmacokinetics*, *20*(5), 309–323.

Painter, L., M. Harding, M. J., & Beeby, P. (1998). Synthesis and interaction with human serum albumin of the first 3, 18-disubstituted derivative of bilirubin. *Journal of Chemical Society, Perkin Transactions 1*, 3041–3044.

Pasvol, G., Weatherall, D. J., Wilson, R. J. M., Smith, D. H., & Gilles, H. M. (1976). Fetal haemoglobin and malaria. *The Lancet*, *307*(7972), 1269–1272.

Peng, X., Sun, Y., Qi, W., Su, R., & He, Z. (2014). Study of the interaction between coenzyme Q 10 and human serum albumin: Spectroscopic approach. *Journal of Solution Chemistry*, *43*(3), 585–607.

Peng, X., Wang, X., Qi, W., Su, R., & He, Z. (2016). Affinity of rosmarinic acid to human serum albumin and its effect on protein conformation stability. *Food Chemistry*, *192*, 178–187.

Peters, T. Jr., (1996). *All about albumin: Biochemistry, genetics, and medical applications*. San Diego: Academic Press.

Peters, T. Jr., & Davidson, L. K. (1982). The biosynthesis of rat serum albumin. *In vivo* studies on the formation of the disulphide bonds. *Journal of Biological Chemistry, 257*(15), 8847–8853.

Pettersen, E. F., Goddard, T. D., Huang, C. C., Couch, G. S., Greenblatt, D. M., Meng, E. C., & Ferrin, T. E. (2004). UCSF Chimera-A visualization system for exploratory research and analysis. *Journal of Computational Chemistry*, *25*, 1605–1612.

Phillips-Howard, P. A., & Wood, D. (1996). The safety of antimalarial drugs in pregnancy. *Drug Safety*, *14*(3), 131–145.

Putnam, F. W. (1975). *The plasma proteins* (2nd ed.). New York: Academic Press.

Quinlan, G. J., Martin, G. S., & Evans, T. W. (2005). Albumin: Biochemical properties and therapeutic potential. *Hepatology, 41*(6), 1211–1219.

Rastegari, B., Karbalaei-Heidari, H. R., Yousefi, R., Zeinali, S., & Nabavizadeh, M. (2016). Interaction of prodigiosin with HSA and β-lactoglobulin: Spectroscopic and molecular docking studies. *Bioorganic and Medicinal Chemistry*, *24*, 1504–1512.

Ranjbar, S., Shokoohinia, Y., Ghobadi, S., Bijari, N., Gholamzadeh, S., Moradi, N., ... Khodarahmi, R. (2013). Studies of the interaction between isoimperatorin and human serum albumin by multispectroscopic method: Identification of possible binding site of the compound using esterase activity of the protein. *The Scientific World Journal*, 2013, Article #305081.

Roche, M., Rondeau, P., Singh, N. R., Tarnus, E., & Bourdon, E. (2008). The antioxidant properties of serum albumin. *FEBS Letters, 582*(13), 1783–1787.

Ross, P. D., & Subramanian, S. (1981). Thermodynamics of protein association reactions: Forces contributing to stability. *Biochemistry*, *20*, 3096–3102.

Ridley, R. G. (2002). Medical need, scientific opportunity and the drive for antimalarial drugs. *Nature*, *415*(6872), 686–693.

Saikia, K., Sravani, Y. D., Ramakrishnan, V., & Chaudhary, N. (2017). Highly potent antimicrobial peptides from N-terminal membrane-binding region of *E. coli* MreB. *Scientific Reports*, *7*(1), 1–9.

Scheider, W., Dintzis, H. M., & Oncley, J. L. (1976). Changes in the electric dipole vector of human serum albumin due to complexing with fatty acids. *Biophysical Journal, 16*(5), 417–431.

Schofield, L. (2002). Antidisease vaccines. *Chemical Immunology*, *80*, 322–342.

Seedher, N., & Bhatia, S. (2005). Mechanism of interaction of the non-steroidal antiinflammatory drugs meloxicam and nimesulide with serum albumin. *Journal of Pharmaceutical and Biomedical Analysis*, *39*(1–2), 257–262.

Sharifi, T., & Ghayeb, Y. (2018). Prediction of the interaction between magnolia extract, herbal medicines, with human serum albumin using molecular dynamics simulation. *Current Bioinformatics*, *13*(2), 207–215.

Sharma, A., & Schulman, S. G. (1999). *Introduction of fluorescence spectroscopy* (1st ed.). New York: Wiley Interscience.

Shrake, A., & Ross, P. D. (1988). Biphasic denaturation of human albumin due to ligand re-distribution during unfolding. *Journal of Biological Chemistry*, *263*, 15392–15399.

Sinclair, D., Zani, B., Donegan, S., Olliaro, P., & Garner, P. (2009). Artemisinin-based combination therapy for treating uncomplicated malaria. *Cochrane Database of Systematic Reviews*, *3*, Article #7483.

Singh, B., Sung, L. K., Matusop, A., Radhakrishnan, A., Shamsul, S. S., Cox-Singh, J., ... & Conway, D. J. (2004). A large focus of naturally acquired *Plasmodium knowlesi* infections in human beings. *The Lancet*, *363*(9414), 1017–1024.

Sirichaiwat, C., Intaraudom, C., Kamchonwongpaisan, S., Vanichtanankul, J., Thebtaranonth, Y., & Yuthavong, Y. (2004). Target guided synthesis of 5-benzyl-2, 4-diamonopyrimidines: Their antimalarial activities and binding affinities to wild type and mutant dihydrofolate reductases from *Plasmodium falciparum*. *Journal of Medicinal Chemistry*, *47*(2), 345–354.

Sudlow, G. D. J. B., Birkett, D. J., & Wade, D. N. (1975). The characterization of two specific drug binding sites on human serum albumin. *Molecular Pharmacology*, *11*(6), 824–832.

Sugio, S., Kashima, A., Mochizuki, S., Noda, M., & Kobayashi, K. (1999). Crystal structure of human serum albumin at 2.5 Å resolution. *Protein Engineering*, *12*(6), 439–446.

Takem, E. N., & D'Alessandro, U. (2013). Malaria in pregnancy. *Mediterranean Journal of Hematology and Infectious Diseases*, *5*(1), Article #*10.*

Tangpukdee, N., Duangdee, C., Wilairatana, P., & Krudsood, S. (2009). Malaria diagnosis: A brief review. *The Korean Journal of Parasitology*, 47, Article #93.

Tayyab, S., Francis, J. A., Kabir, M. Z., Ghani, H., & Mohamad, S. (2019). Probing the interaction of 2,4-dichlorophenoxyacetic acid with human serum albumin as studied by experimental and computational approaches. *Spectrochimica Acta, Part A: Molecular and Biomolecular Spectroscopy*, *207*, 284–293.

Terkuile, F., White, N. J., Holloway, P., Pasvol, G., & Krishna, S. (1993). *Plasmodium falciparum*: *In vitro* studies of the pharmacodynamic properties of drugs used for the treatment of severe malaria. *Experimental Parasitology*, *76*(1), 85–95.

Terkuile, F. O., van Eijk, A. M., & Filler, S. J. (2007). Effect of sulfadoxine-pyrimethamine resistance on the efficacy of intermittent preventive therapy for malaria control during pregnancy: A systematic review. *Journal of the American Medical Association*, *297*(23), 2603–2616.

Terlouw, D. J., Nahlen, B. L., Courval, J. M., Kariuki, S. K., Rosenberg, O. S., Oloo, A. J., ... ter Kuile, F. O. (2003). Sulfadoxine-pyrimethamine in treatment of malaria

in Western Kenya: Increasing resistance and underdosing. *Antimicrobial Agents and Chemotherapy*, *47*(9), 2929–2932.

Trynda-Lemiesz, L. (2004). Paclitaxel-HSA interaction. Binding sites on HSA molecule. *Bioorganic and Medicinal Chemistry*, *12*, 3269–3275.

Tuteja, R. (2007). Malaria− An overview. *The FEBS Journal*, *274*(18), 4670–4679.

Twine, S. M., Gore, M. G., Morton, P., Fish, B. C., Lee, A. G., & East, J. M. (2003). Mechanism of binding of warfarin enantiomers to recombinant domains of human albumin. *Archives of Biochemistry and Biophysics*, *414*(1), 83–90.

Valeur, B. (2009). Molecular Fluorescence. In G. L. Trigg (Ed.), Encyclopedia of applied physics (pp. 477–531). Brookhaven, New York: Wiley-VCH.

Vardanyan, R., & Hruby, V. (2006). *Synthesis of essential drugs* (1st ed.). Arizona, United States: Elsevier.

Wallace, A. C., Laskowski, R. A., & Thornton, J. M. (1995). LIGPLOT: A program to generate schematic diagrams of protein-ligand interactions. *Protein Engineering Design and Selection*, *8*, 127–134.

Wallevik, K. (1973). Reversible denaturation of human serum albumin by pH, temperature, and guanidine hydrocholoride. *Journal of Biological Chemistry, 245*, 2650–2655.

Wani, T. A., Bakheit, A. H., Ansari, M. N., Al-Majed, A. R. A., Al-Qahtani, B. M., & Zargar, S. (2018). Spectroscopic and molecular modeling studies of binding interaction between bovine serum albumin and roflumilast. *Drug Design, Development and Therapy*, *12*, 2627–2634.

Whegang, S. Y., Tahar, R., Foumane, V. N., Soula, G., Gwét, H., Thalabard, J. C., & Basco, L. K. (2010). Efficacy of non-artemisinin-and artemisinin-based combination therapies for uncomplicated *falciparum* malaria in Cameroon. *Malaria Journal*, *9*(1), Article #56.

White, N. J. (1997). Assessment of the pharmacodynamic properties of antimalarial drugs *in vivo*. *Antimicrobial Agents and Chemotherapy*, *41*(7), Article #1413.

World Health Organization. (2000). *The World Health Report 2000: Health Systems: Improving performance*. Geneva, Switzerland.

World Health Organization. (2018). *High Burden to High Impact: A targeted malaria response* (No. WHO/CDS/GMP/2018.25 Rev. 1).

World Health Organization. (2020). Eleventh meeting of the WHO Vector Control Advisory Group: Meeting Report, Geneva, 11–13, November 2019.

Wu, J., Shu-Yun, B., Xiao-Yue, S., Zhao, R., Ji-Hong, W., & Hui-Feng, Z. (2019). Study on the interaction of fisetholz with BSA/HSA by multispectroscopic, cyclic voltammetric, and molecular docking technique. *Journal of Biomolecular Structure and Dynamics*, *37*, 3496–3505.

Wu, D., Liu, D., Zhang, Y., Zhang, Z., & Li, H. (2018). Unravelling the binding mechanism of benproperine with human serum albumin: A docking, fluorometric, and thermodynamic approach. *European Journal of Medicinal Chemistry*, *146*, 245–250.

Yadav, P., Sharma, B., Sharma, C., Singh, P., & Awasthi, S. K. (2020). Interaction between the antimalarial drug dispiro-tetraoxanes and human serum albumin: A combined study with spectroscopic methods and computational studies. *ACS Omega*, *5*(12), 6472–6480.

Yamasaki, K., Chuang, V. T. G., Maruyama, T., & Otagiri, M. (2013). Albumin–drug interaction and its clinical implication. *Biochimica et Biophysica Acta - General Subjects*, *1830*(12), 5435–5443.

Yang, J., Jing, Z. H., Jie, J. J., & Guo, P. (2009). Fluorescence spectroscopy study on the interaction between gossypol and bovine serum albumin. *Journal of Molecular Structure*, *920*(1–3), 227–230.

Yeggoni, D. P., Kuehne, C., Rachamallu, A., & Subramanyam, R. (2017). Elucidating the binding interaction of andrographolide with the plasma proteins: Biophysical and computational approach. *RSC Advances*, *7*(9), 5002–5012.

Yuan, L., Liu, M., Sun, B., Liu, J., Wei, X., Wang, Z., ... Han, J. (2017). Calorimetric and spectroscopic studies on the competitive behavior between (−)- epigallocatechin-3-gallate and 5-fluorouracil with human serum albumin. *Journal of Molecular Liquids*, *248*, 330–339.

Zhivkova, Z. (2015). Studies on drug–human serum albumin binding: The current state of the matter. *Current Pharmaceutical Design*, *21*(14), 1817–1830.

Zsila, F. (2013). Circular dichroism spectroscopic detection of ligand binding induced subdomain IB specific structural adjustment of human serum albumin. *Journal of Physical Chemistry B*, *117*(37), 10798–10806.

Zunszain, P. A., Ghuman, J., Komatsu, T., Tsuchida, E., & Curry, S. (2003). Crystal structural analysis of human serum albumin complexed with hemin and fatty acid. *BMC Structural Biology*, *3*(1), 1–9.

LIST OF PUBLICATION AND PRESENTATION

List of publication

1. **Francis, J. A**., Shalauddin, M., Ridzwan, N. F. W., Mohamad, S. B., Basirun, W. J., & Tayyab, S. (2020). Interaction mechanism of an antimalarial drug, sulfadoxine with human serum albumin. *Spectroscopy Letters*, *53*(5)*,* 391–405.

Presentation

1. **Francis, J. A**., Shalauddin, M., Ridzwan, N. F. W., Mohamad, S. B., Basirun, W. J., & Tayyab, S. (2019). *Understanding molecular interaction between sulfadoxine and human serum albumin through multispectroscopic, voltammetric and molecular docking methods.* Poster presented at the 24th Biological Sciences Graduate Congress (BSGC) 2019, held on 19th & 20th December 2019 at the University of Malaya. Abstract No. P21, page 103. (awarded 2nd Runner-Up prize for the Poster Presentation).